Forum Inżynierii Materiałowej

Materials Engineering Forum

Self-lubricating surface layers and composite materials produced by laser alloying and powder metallurgy

29.11.2023

Dr. Eng. Adam Piasecki

Institute of Materials Science and Engineering, Faculty of Materials Engineering and Technical Physics, Poznan University of Technology
adam.piasecki@put.poznan.pl

Wear is the main cause of around **80%** exhaustion of the operational potential of machines and vehicles. In the case of mating parts, it is important to lubricate them.

Conducting effective lubrication of the contact surfaces of mating parts is an effective method to counteract friction and reduce their wear.

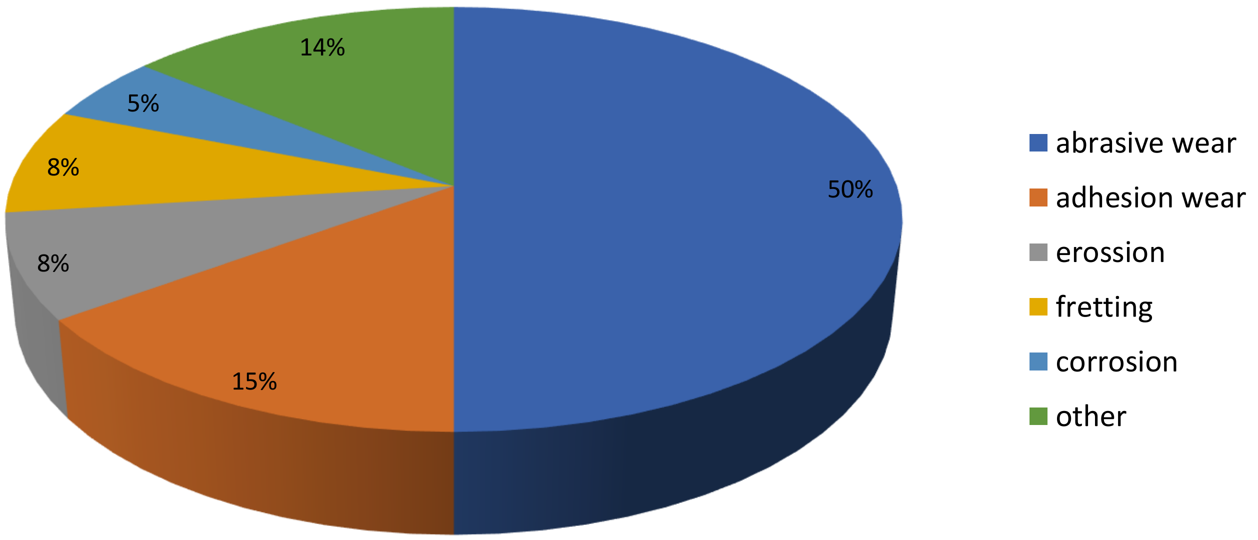

The production of self-lubricating wear-resistant materials containing solid lubricants **can be one of the most effective and economical methods** to increase the durability of machine and vehicles parts.

Solid lubricants

Soft metals	Au, Ag, Sn, Pb, Zn
Sulfides	MoS_2, WS_2
Carbon	Graphite, CNTs
Polymers	PTFE
Oxides	ZnO, PbO, TiO_2
Fluorides	CaF_2, BaF_2
Salts	$CaSO_4$, $BaSO_4$

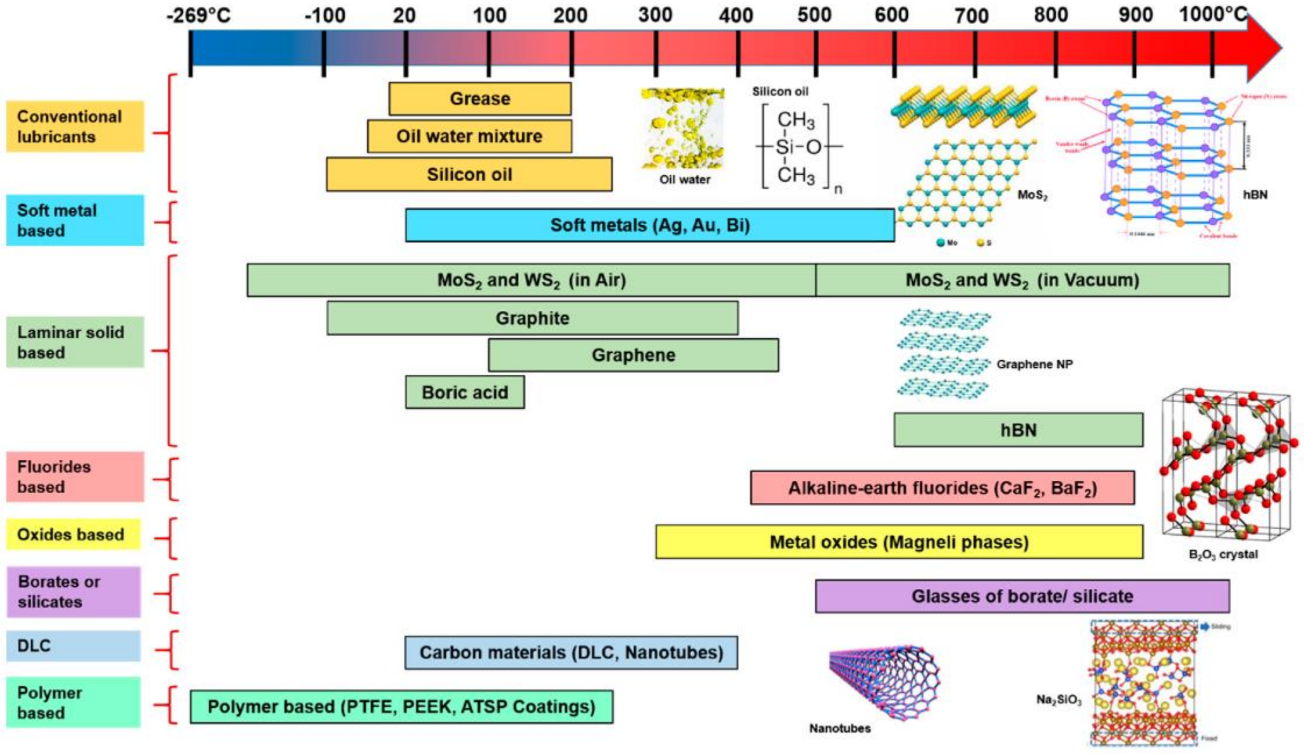

A graphical representation of effective temperature ranges for solid-lubricating materials (solid lubricants),

Kumar, R.; Hussainova, I.; Rahmani, R.; Antonov, M. Solid Lubrication at High-Temperatures—A Review. *Materials* **2022**, *15*, 1695. *https://doi.org/10.3390/ma15051695*

Powders

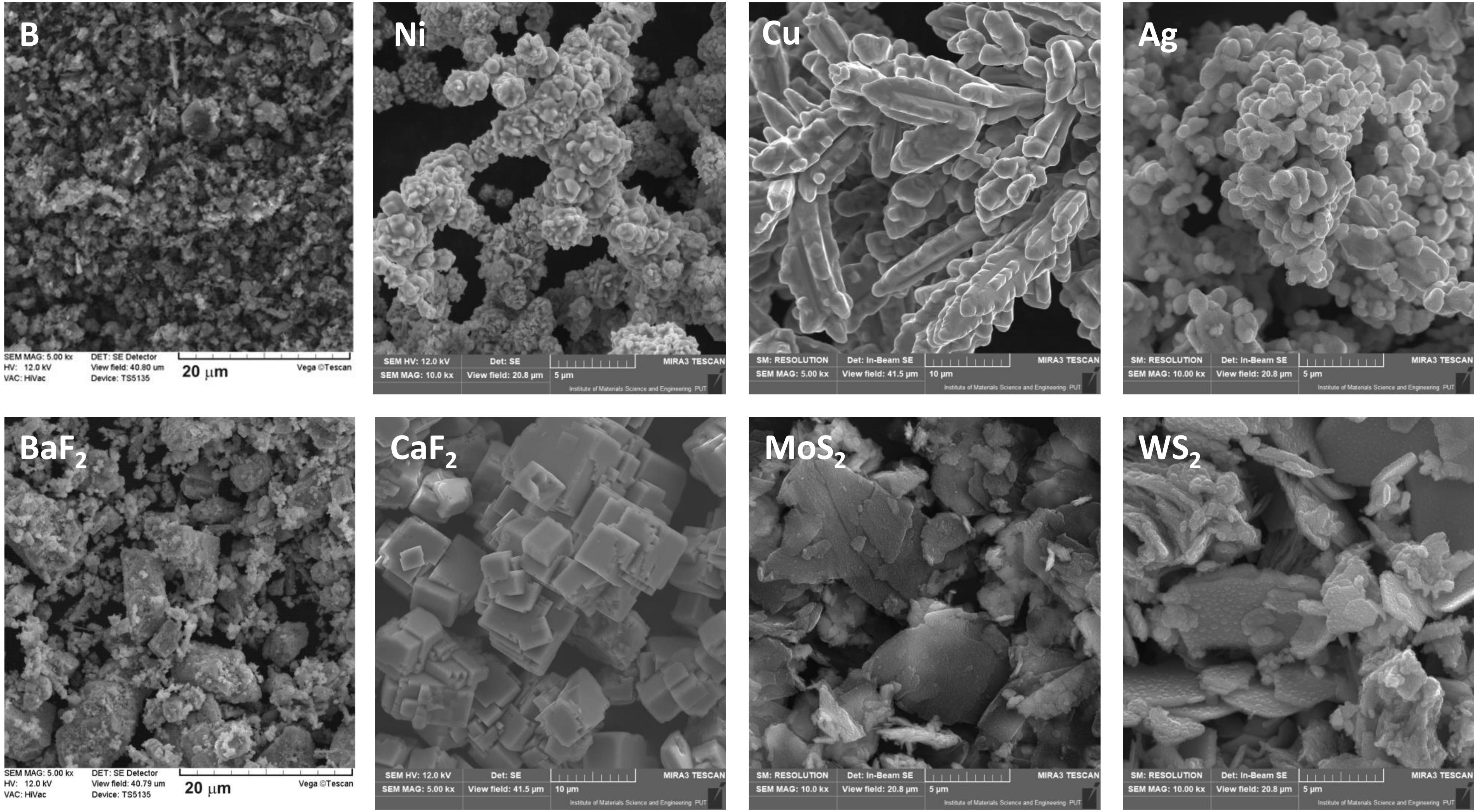
B
Ni
Cu
Ag
BaF_2
CaF_2
MoS_2
WS_2
20 µm
5 µm
10 µm
5 µm
20 µm
10 µm
5 µm
5 µm

Powders - oxides

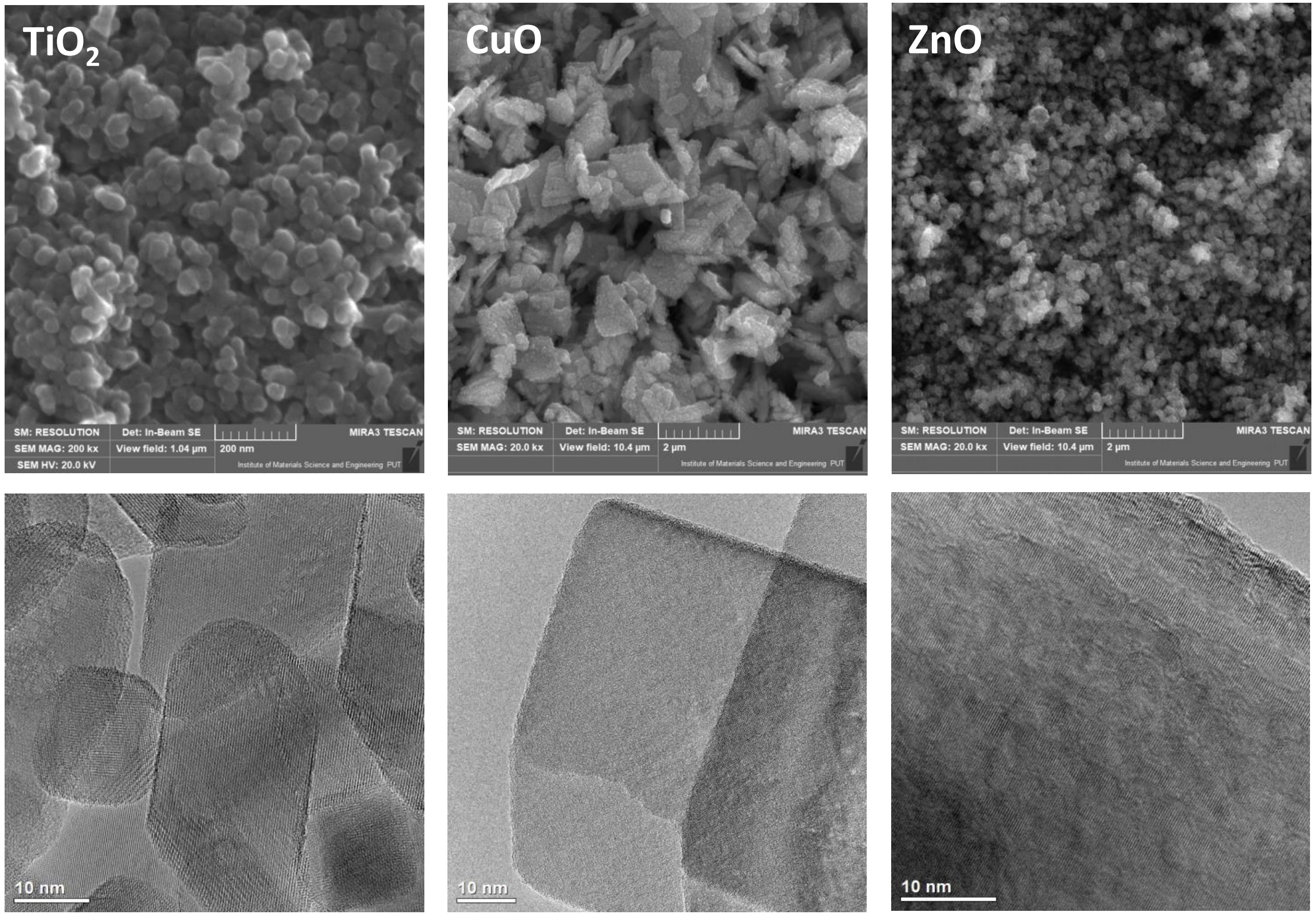

Powders - MWCNTs

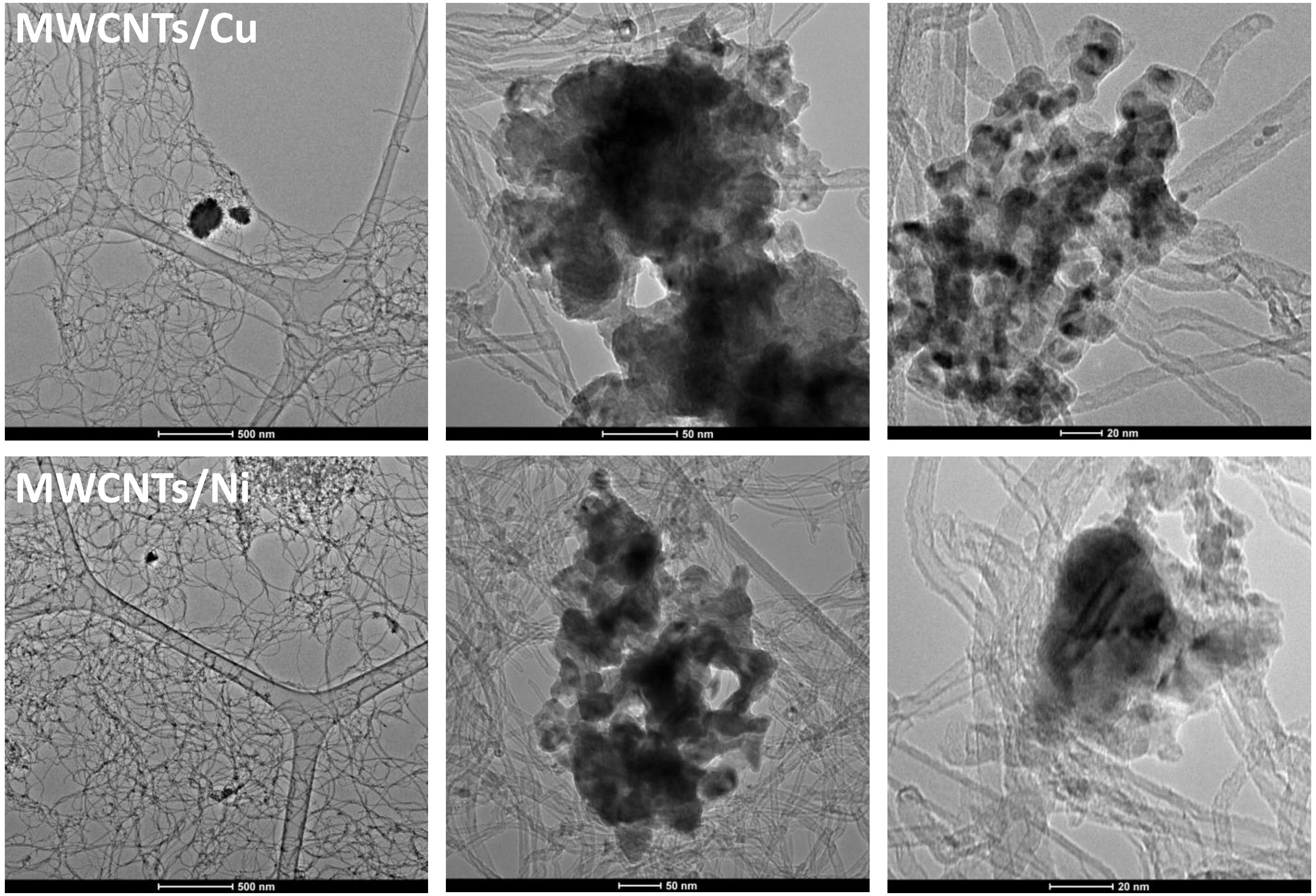

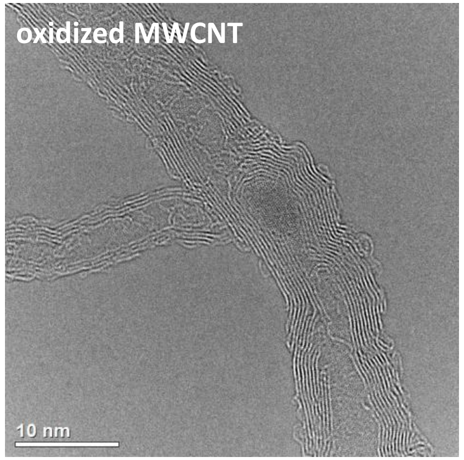

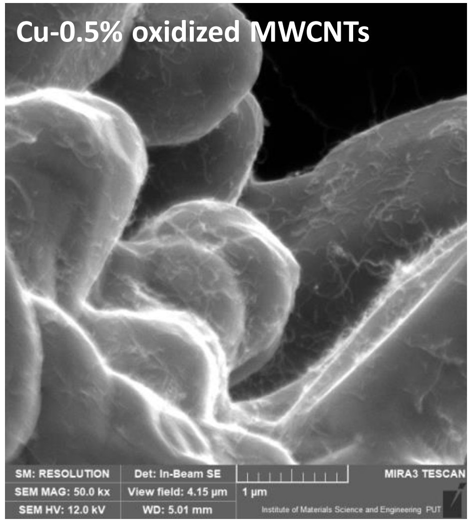

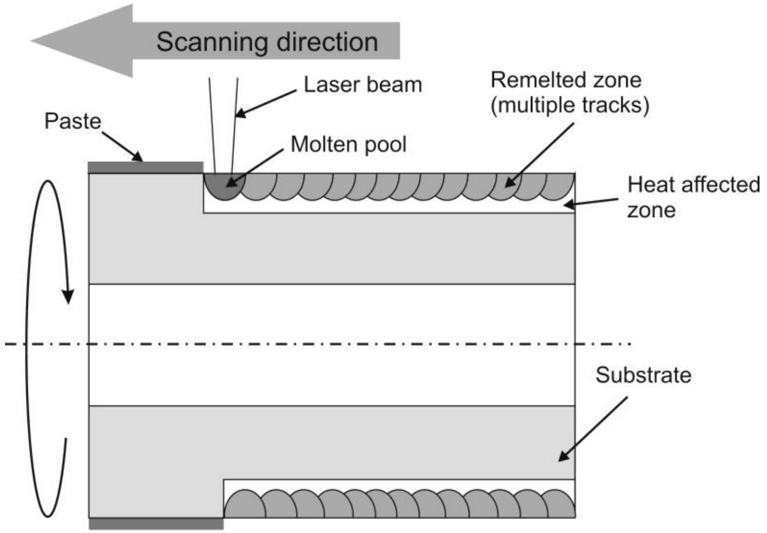

Scheme of two-step method of laser-alloying

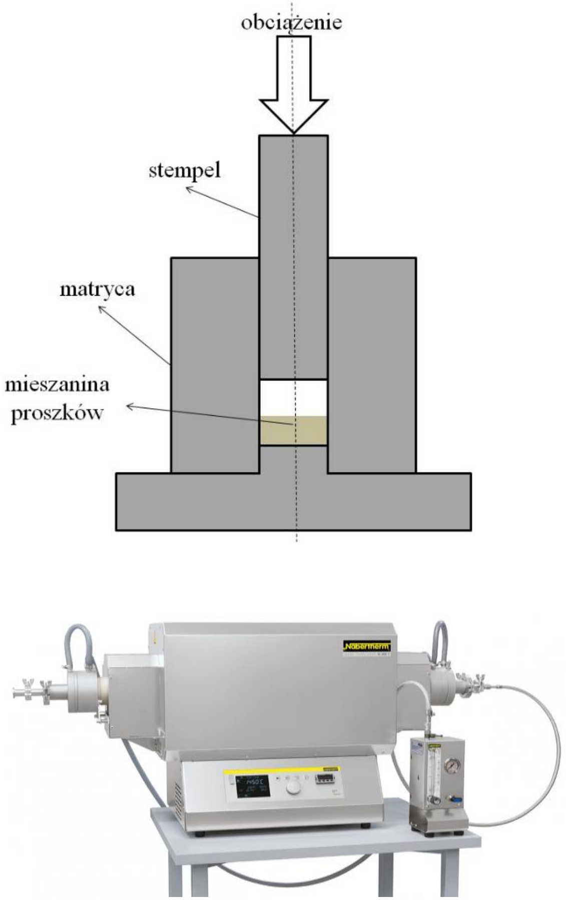

Scheme of producing sintered composite materials

HP D 25/3 (FCT Systeme, Germany, FAST/SPS method), Łukasiewicz Research Network - Poznań

Piasecki A., Kotkowiak M., Makuch N., Kulka M., Wear behavior of self-lubricating boride layers produced on Inconel 600-alloy by laser alloying, Wear, 2019, 426-427, pp. 919-933.
Piasecki A., Paczos P., Tuliński M., Kotkowiak M., Popławski M., Jakubowicz M., Boncel S., Marek A.A., Buchwald T., Gapiński B., Terzyk A.P., Korczeniewski E., Wieczorowski M., Microstructure, mechanical properties and tribological behavior of Cu-nano TiO2-MWCNTs composite sintered materials. Wear 2023, vol. 522, s. 204834-1-204834-16,

Self-lubricating surface layers and composite materials produced by laser alloying and powder metallurgy

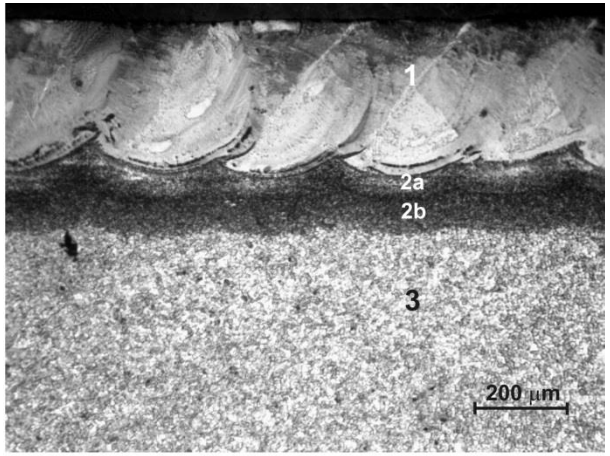

Microstructure of laser-alloyed 100CrMnSi6-4 steel with boron

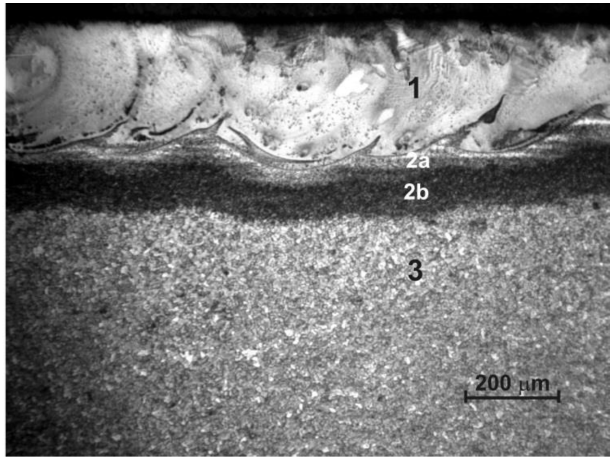

Microstructure of laser-alloyed 100CrMnSi6-4 steel with boron and CaF_2

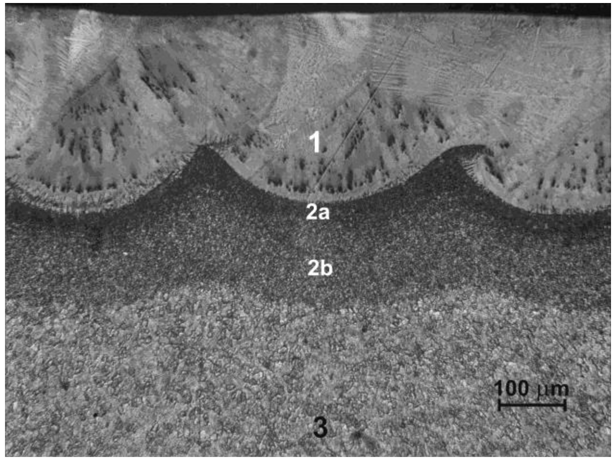

Microstructure of laser-alloyed 100CrMnSi6-4 steel with boron and BaF_2

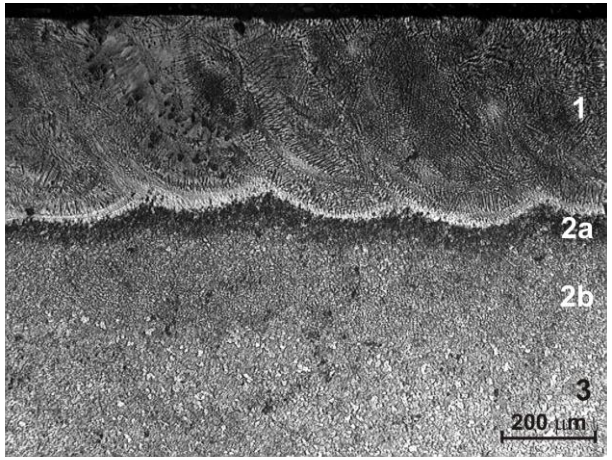

Microstructure of laser-alloyed 100CrMnSi6-4 steel with boron, CaF_2, and BaF_2

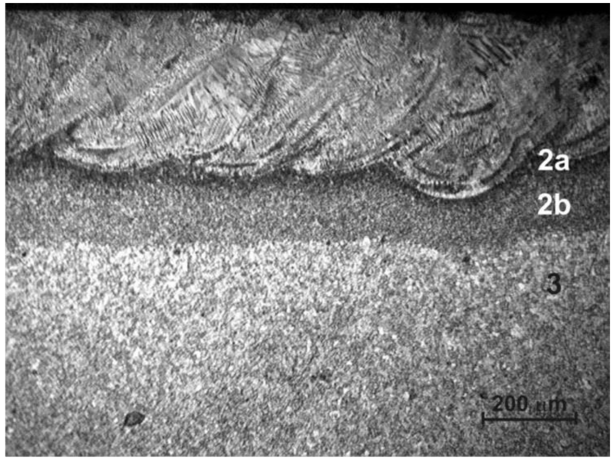

Microstructure of laser-alloyed 100CrMnSi6-4 steel with boron and 20% CaF_2

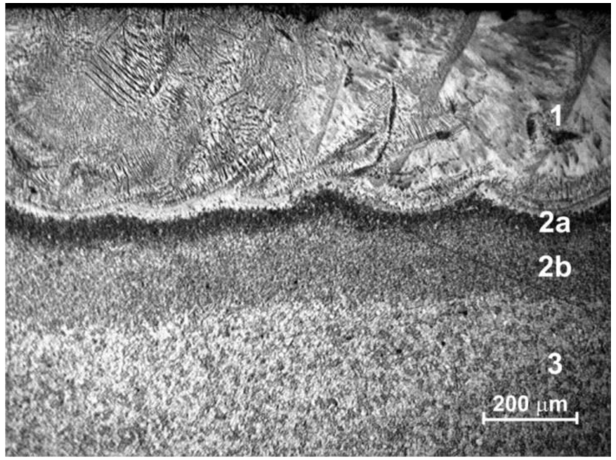

Microstructure of laser-alloyed 100CrMnSi6-4 steel with boron and 20% BaF_2

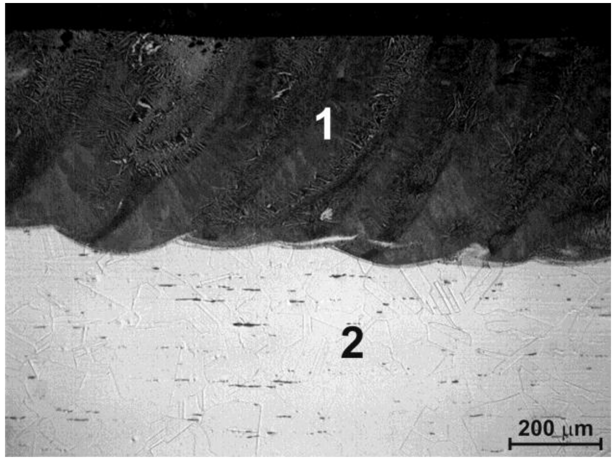

Microstructure of laser-alloyed 316L steel with boron and CaF_2

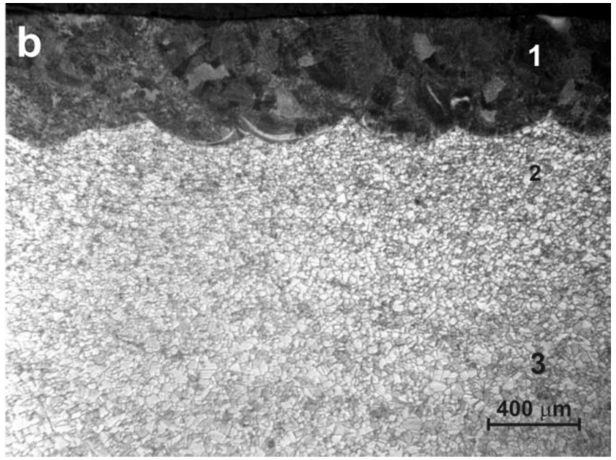

Microstructure of laser-alloyed Inconel®600 alloy with boron and CaF_2

1 – remelted zone; 2 – heat-affected zone; 3 – substrate

Piasecki A., Kulka, M., Kotkowiak, M., Wear resistance improvement of 100CrMnSi6-4 bearing steel by laser boriding using CaF_2 self-lubricating addition, Tribology International, vol. 97, 2016, s. 173-191.
Piasecki A., Kotkowiak M., Kulka M., Self-lubricating surface layers produced using laser alloying of bearing steel, Wear, 2017, 376-377, pp. 993-1008.
Piasecki A., Kotkowiak M., Kulka M., Laser boridnig of 100CrMnSi6-4 steel using BaF_2 self-lubricating addition, Inżynieria Materiałowa, 2017, 3, s.143-148.
Mikołajczak D., **Piasecki A.**, Kulka M., Makuch N., Laser alloying of 316L steel with boron using CaF_2 self-lubricating addition, Inżynieria Materiałowa Materials Engineering, 1 (209), 2016, s.4-9.
Piasecki A., Kotkowiak M., Kulka M., The effect of CaF_2 and BaF_2 solid lubricants on wear resistance of laser-borided 100CrMnSi6-4 bearing steel, Archives of Materials Science and Engineering, 2017, 86(1), pp. 15-23.
Piasecki A., Kotkowiak M., Makuch N., Kulka M., Wear behavior of self-lubricating boride layers produced on Inconel 600-alloy by laser alloying, Wear, 2019, 426-427, pp. 919-933.

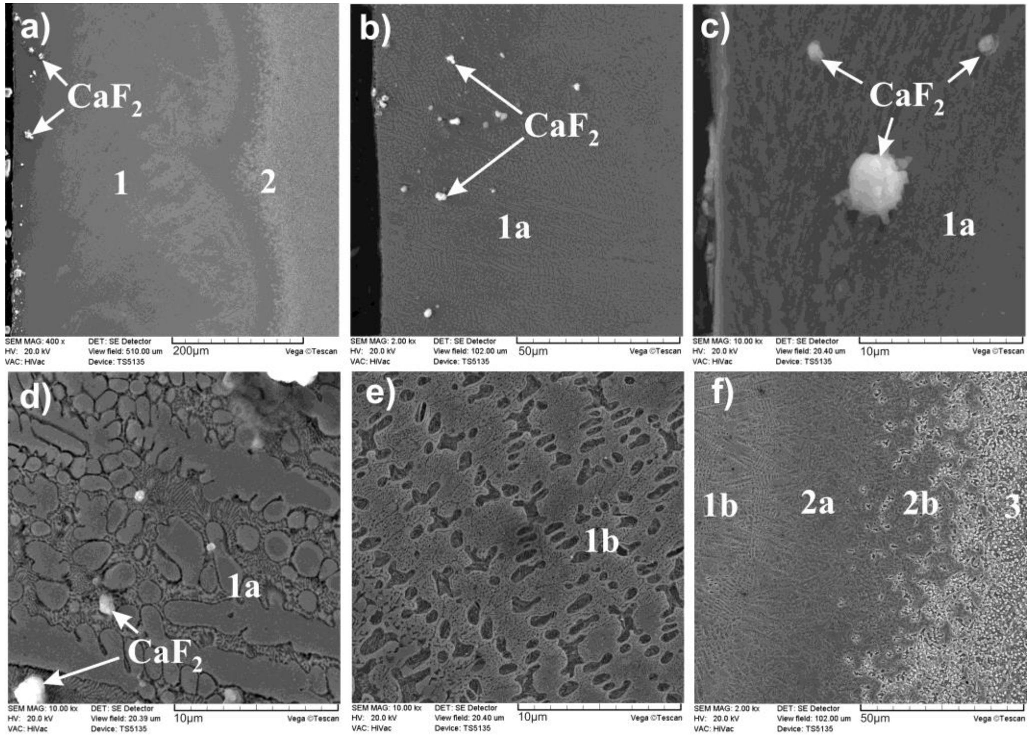

SE images of laser-borided layer with CaF_2 produced on 100CrMnSi6-4 steel (P = 1.17 kW).

Element	Wt%	At%
Ca	2.79	2.05
Fe	74.90	39.39
Cr	0.40	0.23
F	1.01	1.57
B	20.90	56.77
Total	100.00	100.00

Element	Wt%	At%
Ca	0.31	0.24
Fe	79.44	44.42
Cr	1.39	0.84
B	18.87	54.50
Total	100.00	100.00

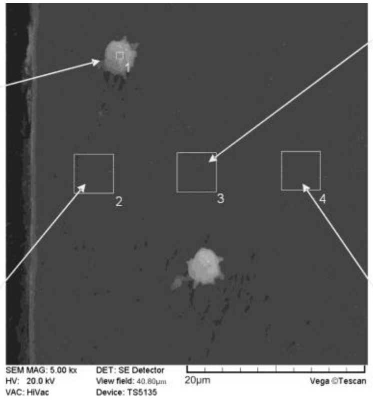

Element	Wt%	At%
Ca	0.09	0.07
Fe	80.50	45.91
Cr	1.36	0.83
B	18.05	53.19
Total	100.00	100.00

Element	Wt%	At%
Ca	0.09	0.07
Fe	80.98	46.72
Cr	1.36	0.84
B	17.57	52.37
Total	100.00	100.00

Results of X-ray microanalysis of laser-borided 100CrMnSi6-4 steel with CaF_2

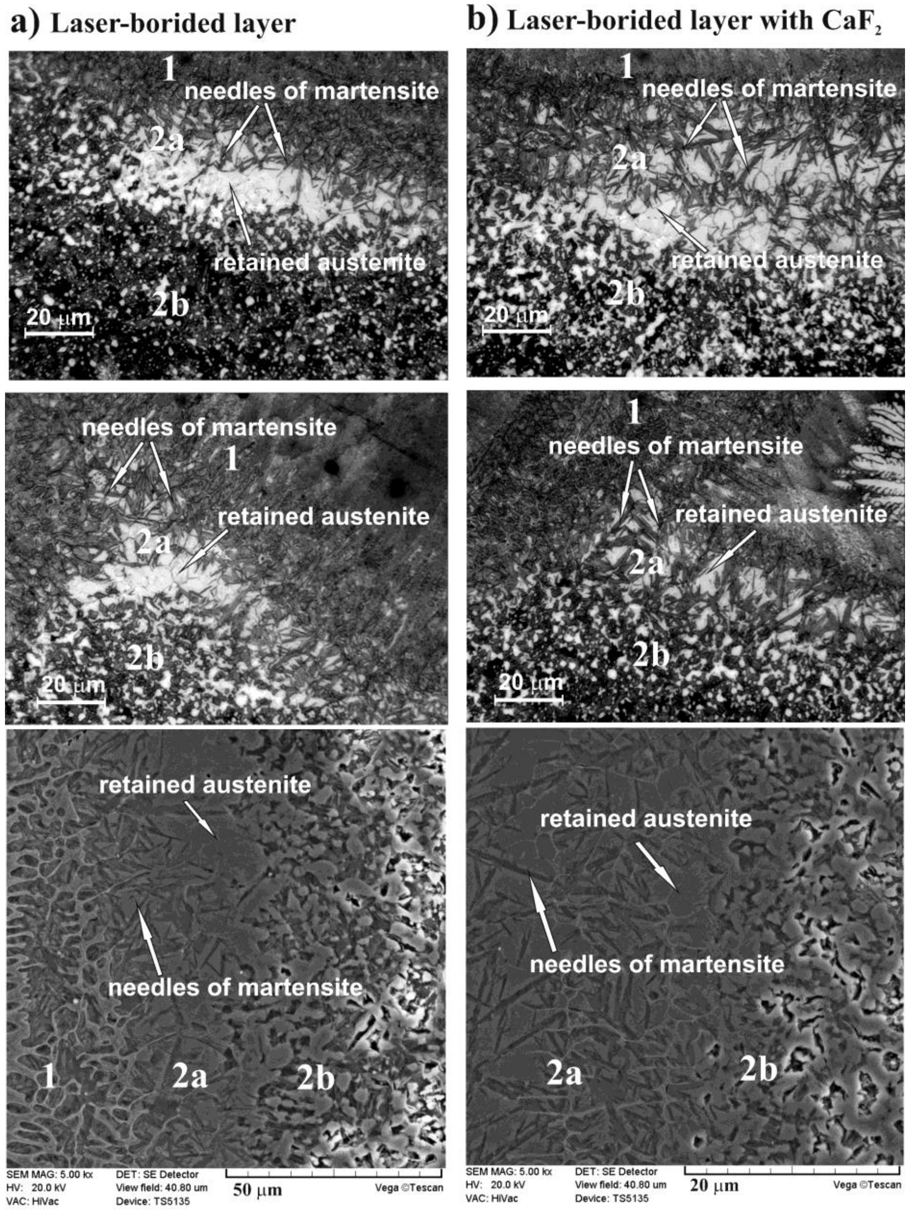

OM and SE images of heat-affected zone in laser-borided layer (a) and in laser-borided layer with CaF_2 (b)

Piasecki A., Kulka, M., Kotkowiak, M., Wear resistance improvement of 100CrMnSi6-4 bearing steel by laser boriding using CaF_2 self-lubricating addition, Tribology International, vol. 97, 2016, s. 173-191.

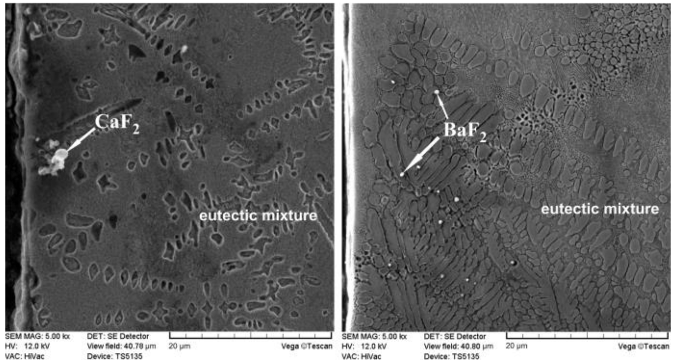

SE images of laser-alloyed layers with boron and CaF_2 (a) and with boron and BaF_2 (b). (P = 1.43 kW)

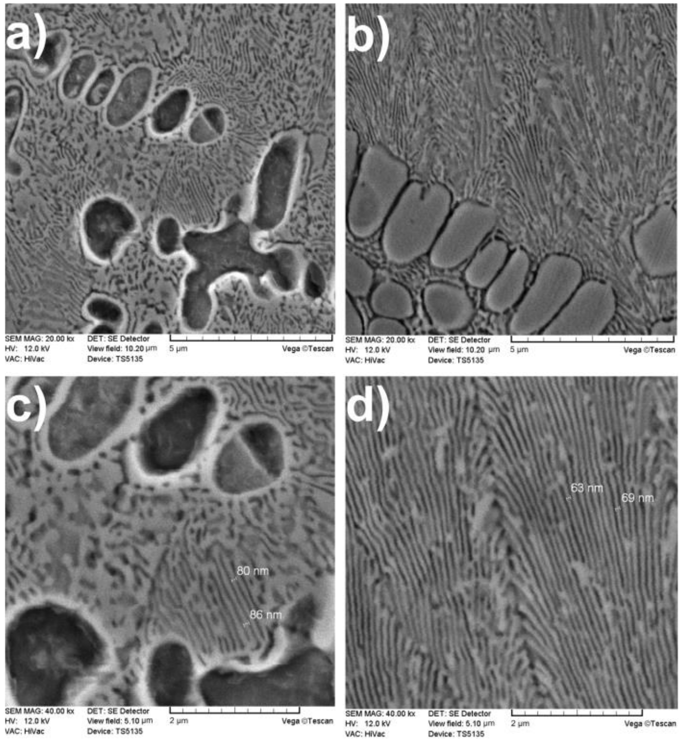

SE images of eutectic mixture with a nanometric components of structure of laser-alloyed layers with boron and CaF_2 (a, c) and with boron and BaF_2 (b, d).

Element	Wt%
Ca	3.08
Cr	1.31
Fe	62.59
B	33.03
Total	100

Element	Wt%
Ca	0.00
Cr	1.52
Fe	74.25
B	24.23
Total	100

Element	Wt%
Ca	0.93
Cr	1.49
Fe	64.36
B	33.22
Total	100

Element	Wt%
Ca	0.03
Cr	1.01
Fe	71.52
B	27.44
Total	100

Results of X-ray microanalysis on the fracture of laser-alloyed 100CrMnSi6-4 steel with boron and CaF_2

Element	Wt%
Ba	75.18
Cr	0.00
Fe	5.79
B	19.03
Total	100

Element	Wt%
Ba	0.00
Cr	1.54
Fe	72.48
B	25.98
Total	100

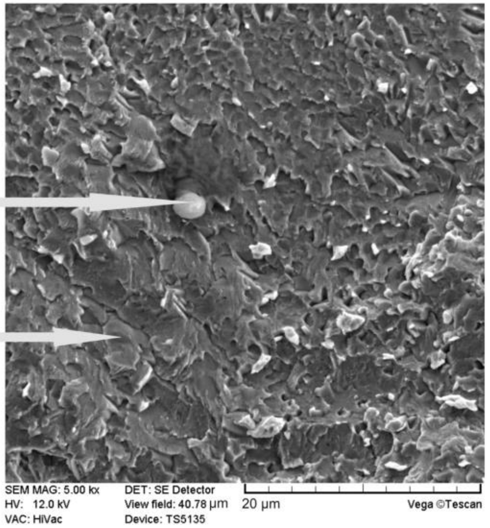

Results of X-ray microanalysis on the fracture of laser-alloyed 100CrMnSi6-4 steel with boron and BaF_2

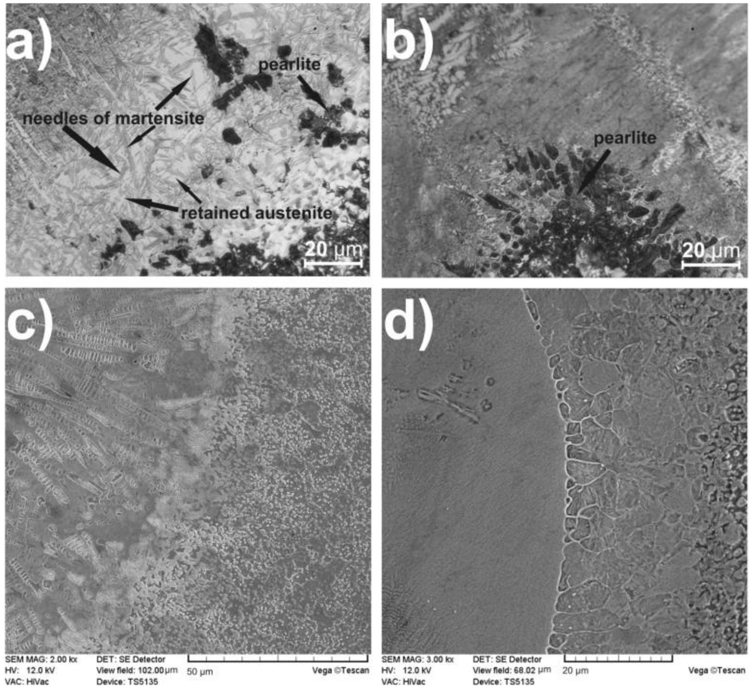

OM and SE images of heat-affected zone in laser-alloyed layer with boron and CaF_2 (a, c) and in laser-alloyed layer with boron and BaF_2 (b,d).

Piasecki A., Kotkowiak M., Kulka M., Self-lubricating surface layers produced using laser alloying of bearing steel, Wear, 2017, 376-377, pp. 993-1008.

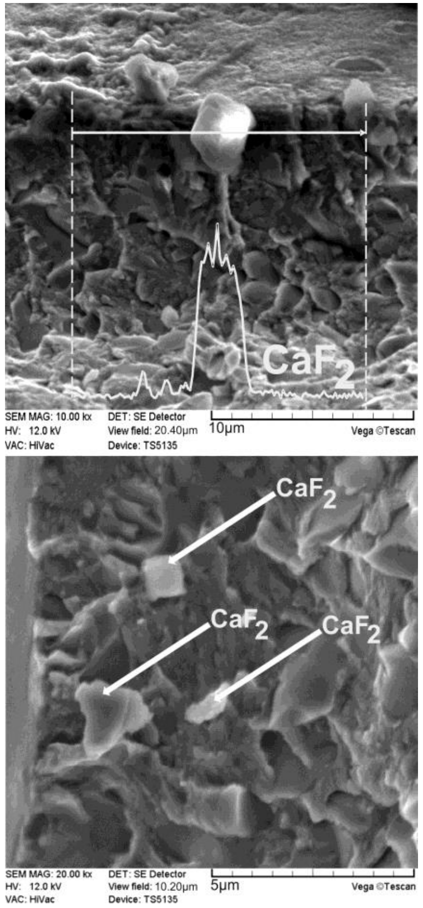

Fractures of laser-alloyed layers with boron and 10%CaF_2

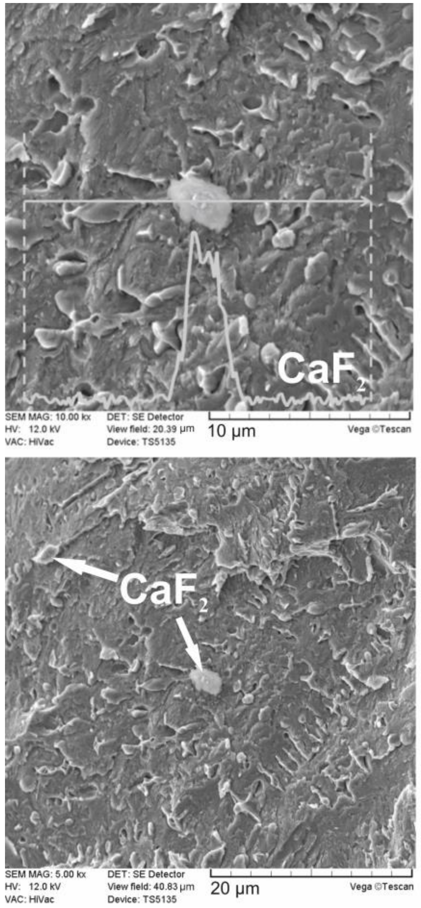

Fractures of laser-alloyed layers with boron and 20%CaF_2

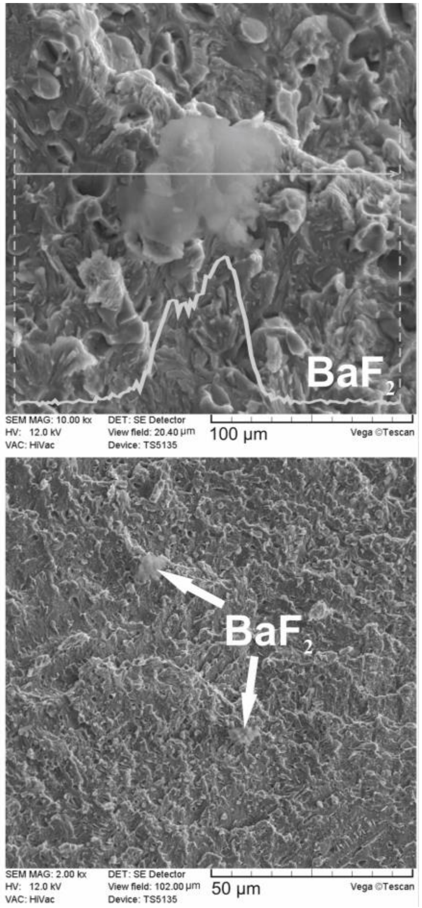

Fractures of laser-alloyed layers with boron and 20%BaF_2

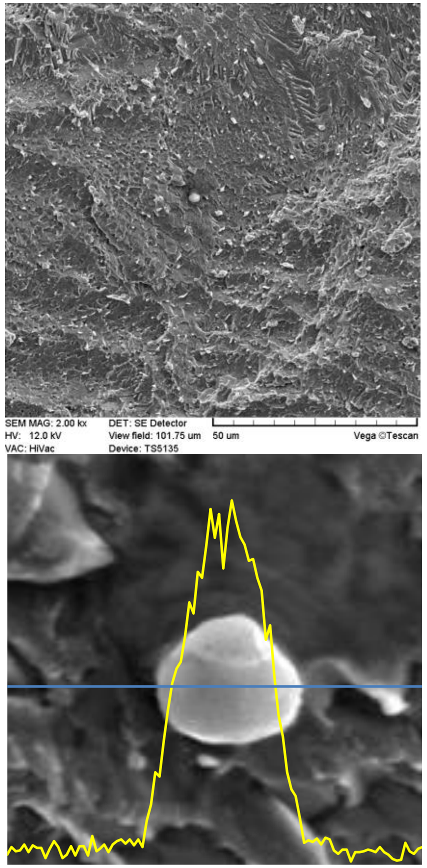

Fractures of laser-alloyed layers with boron and BaF_2

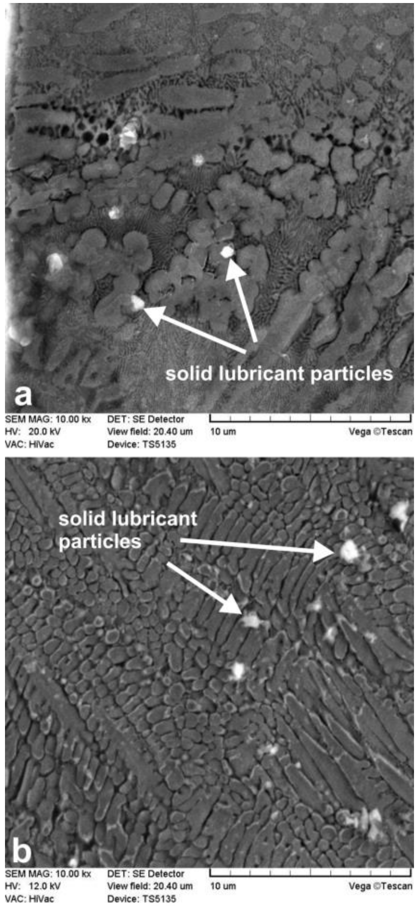

Fractures of laser-alloyed layers with boron, CaF_2, and BaF_2

Piasecki A., Kulka, M., Kotkowiak, M., Wear resistance improvement of 100CrMnSi6-4 bearing steel by laser boriding using CaF2 self-lubricating addition, Tribology International, vol. 97, 2016, s. 173-191.
Piasecki A., Kotkowiak M., Kulka M., Self-lubricating surface layers produced using laser alloying of bearing steel, Wear, 2017, 376-377, pp. 993-1008.
Piasecki A., Kotkowiak M., Kulka M., Laser boridnig of 100CrMnSi6-4 steel using BaF2 self-lubricating addition, Inżynieria Materiałowa, 2017, 3, s.143-148.
Piasecki A., Kotkowiak M., Kulka M., The effect of CaF2 and BaF2 solid lubricants on wear resistance of laser-borided 100CrMnSi6-4 bearing steel, Archives of Materials Science and Engineering, 2017, 86(1), pp. 15-23.

non-eatched eatched

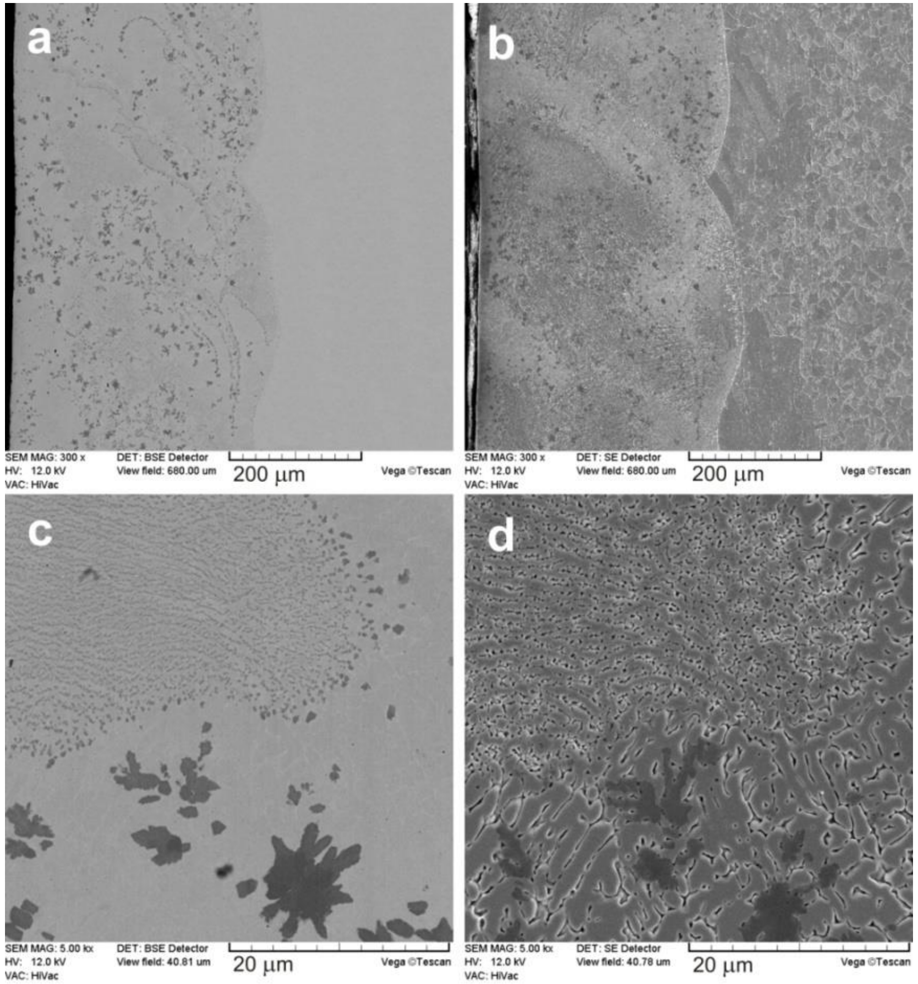

SEM microstructure of laser-alloyed Inconel®600 alloy with boron and CaF_2 at laser beam power of 1.56 kW based on BSE images (a, c) and SE images (b, d).

non-eatched eatched

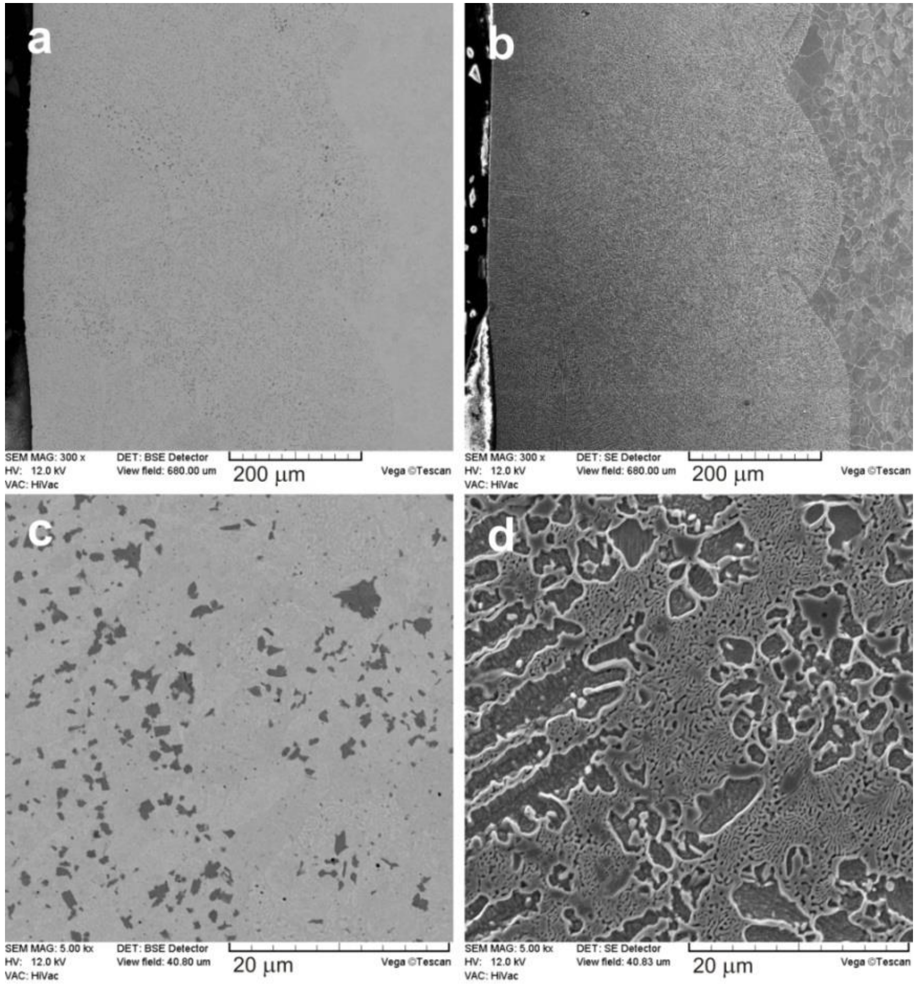

SEM microstructure of laser-alloyed Inconel®600 alloy with boron and CaF_2 at laser beam power of 1.95 kW based on BSE images (a, c) and SE images (b, d).

Piasecki A., Kotkowiak M., Makuch N., Kulka M., Wear behavior of self-lubricating boride layers produced on Inconel 600-alloy by laser alloying, Wear, 2019, 426-427, pp. 919-933.

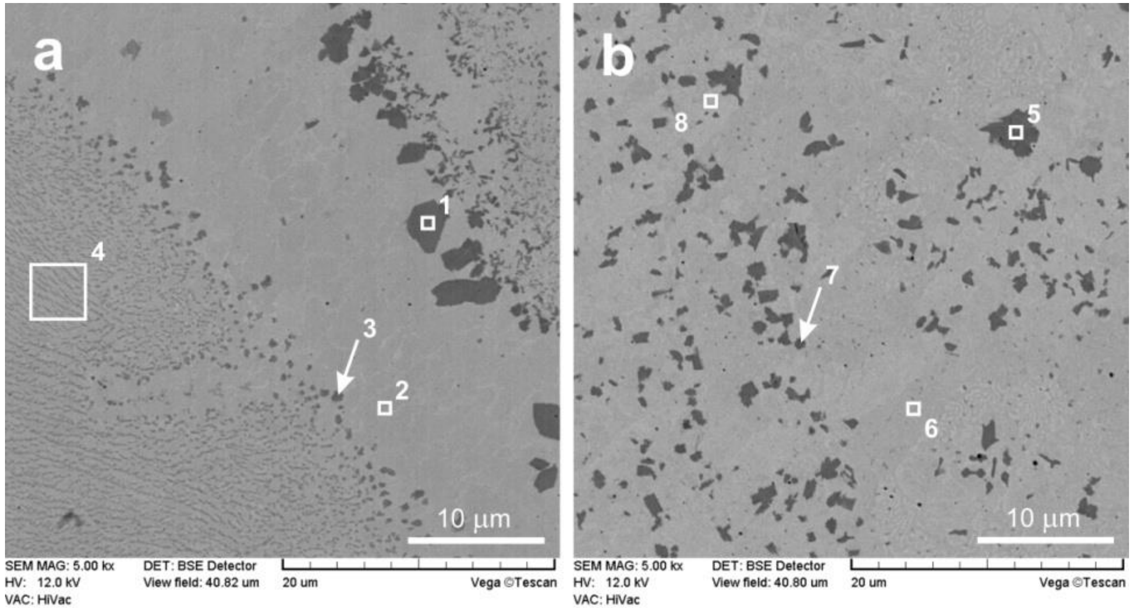

SEM microstructure in the contrast of backscattered electrons (BSE) and areas of X-ray microanalysis of laser-alloyed Inconel®600-alloy with boron and CaF_2 at laser beam power of 1.56 kW (a) and 1.95 kW (b).

EDS X-ray microanalysis of Inconel®600-alloy after laser alloying with boron and CaF_2

Spot	Element. wt%				
	B	Ca	Cr	Fe	Ni
1	12.99	0.16	75.36	5.04	6.45
2	11.27	0.04	13.19	7.35	68.15
3	13.99	0.14	49.19	7.1	29.58
4	11.97	0.03	14.28	7.48	66.23
5	13.44	0.13	78.56	2.94	4.92
6	17.96	0.01	8.91	5.79	67.33
7	15.04	0.18	63.51	3.52	17.75
8	13.72	0.04	11.47	9.05	65.71

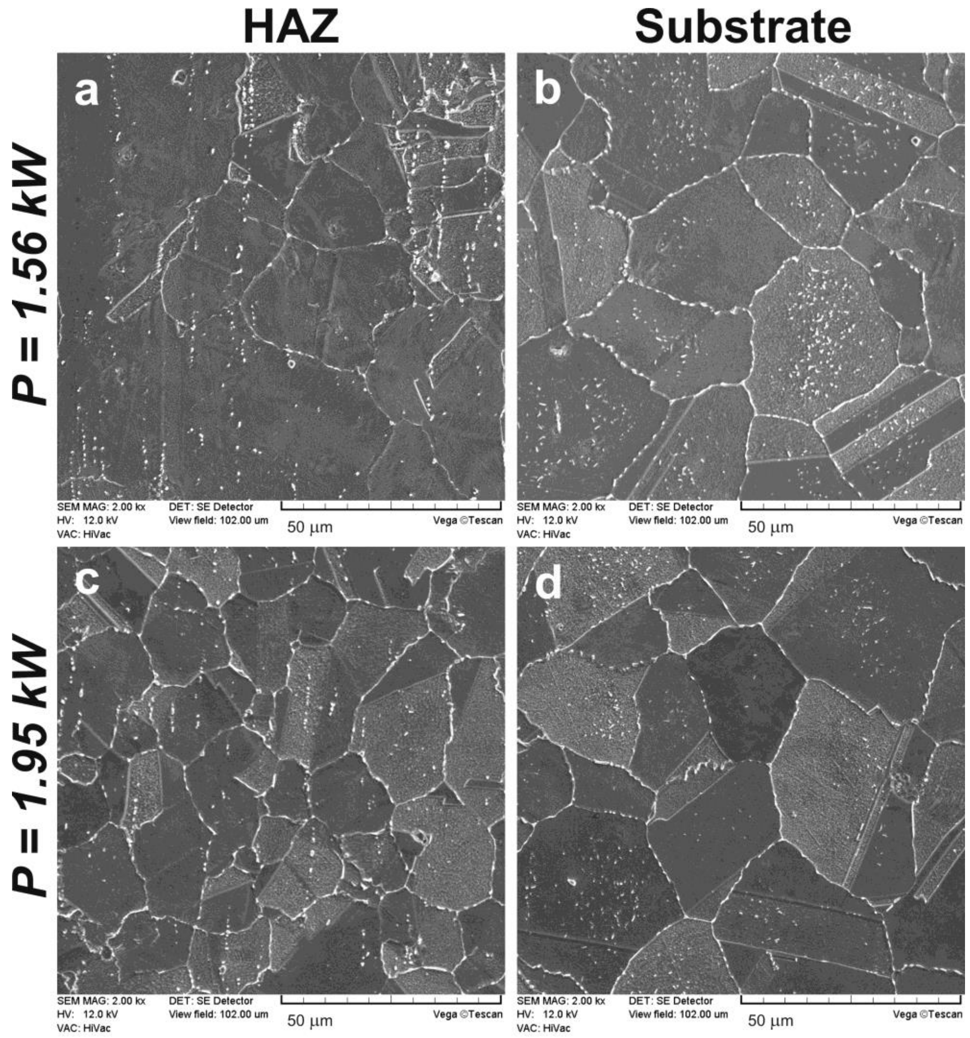

SEM microstructure of the HAZ and the substrate at laser beam power of 1.56 kW (a,b) and 1.95 kW (c,d).

Piasecki A., Kotkowiak M., Makuch N., Kulka M., Wear behavior of self-lubricating boride layers produced on Inconel 600-alloy by laser alloying, Wear, 2019, 426-427, pp. 919-933.

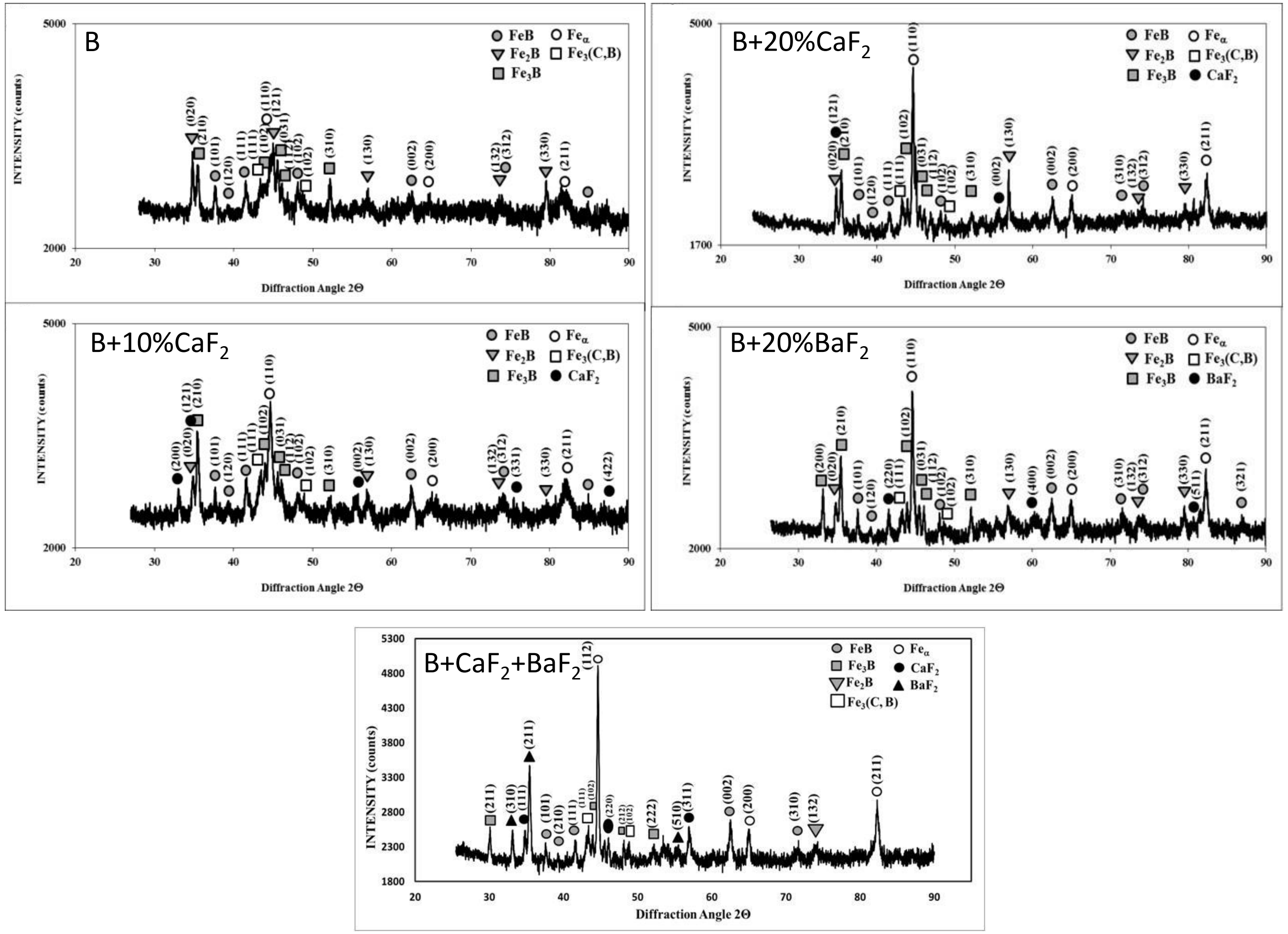

XRD Patterns of laser-alloyed 100CrMnSi6-4 steel

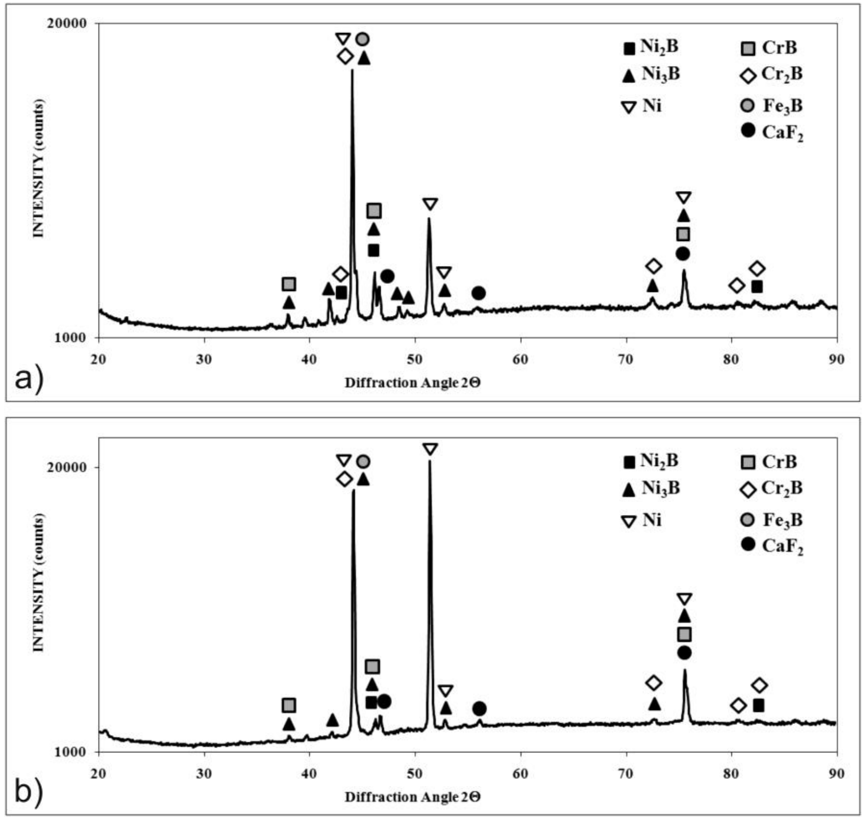

XRD Patterns of laser-alloyed Inconel®600 alloy with B and CaF_2 at laser beam power of 1.56 kW (a) and 1.95 kW (b).

Piasecki A., Kulka, M., Kotkowiak, M., Wear resistance improvement of 100CrMnSi6-4 bearing steel by laser boriding using CaF_2 self-lubricating addition, Tribology International, vol. 97, 2016, s. 173-191.
Piasecki A., Kotkowiak M., Kulka M., Self-lubricating surface layers produced using laser alloying of bearing steel, Wear, 2017, 376-377, pp. 993-1008.
Piasecki A., Kotkowiak M., Kulka M., The effect of CaF_2 and BaF_2 solid lubricants on wear resistance of laser-borided 100CrMnSi6-4 bearing steel, Archives of Materials Science and Engineering, 2017, 86(1), pp. 15-23.
Piasecki A., Kotkowiak M., Makuch N., Kulka M., Wear behavior of self-lubricating boride layers produced on Inconel 600-alloy by laser alloying, Wear, 2019, 426-427, pp. 919-933.

Self-lubricating surface layers and composite materials produced by laser alloying and powder metallurgy

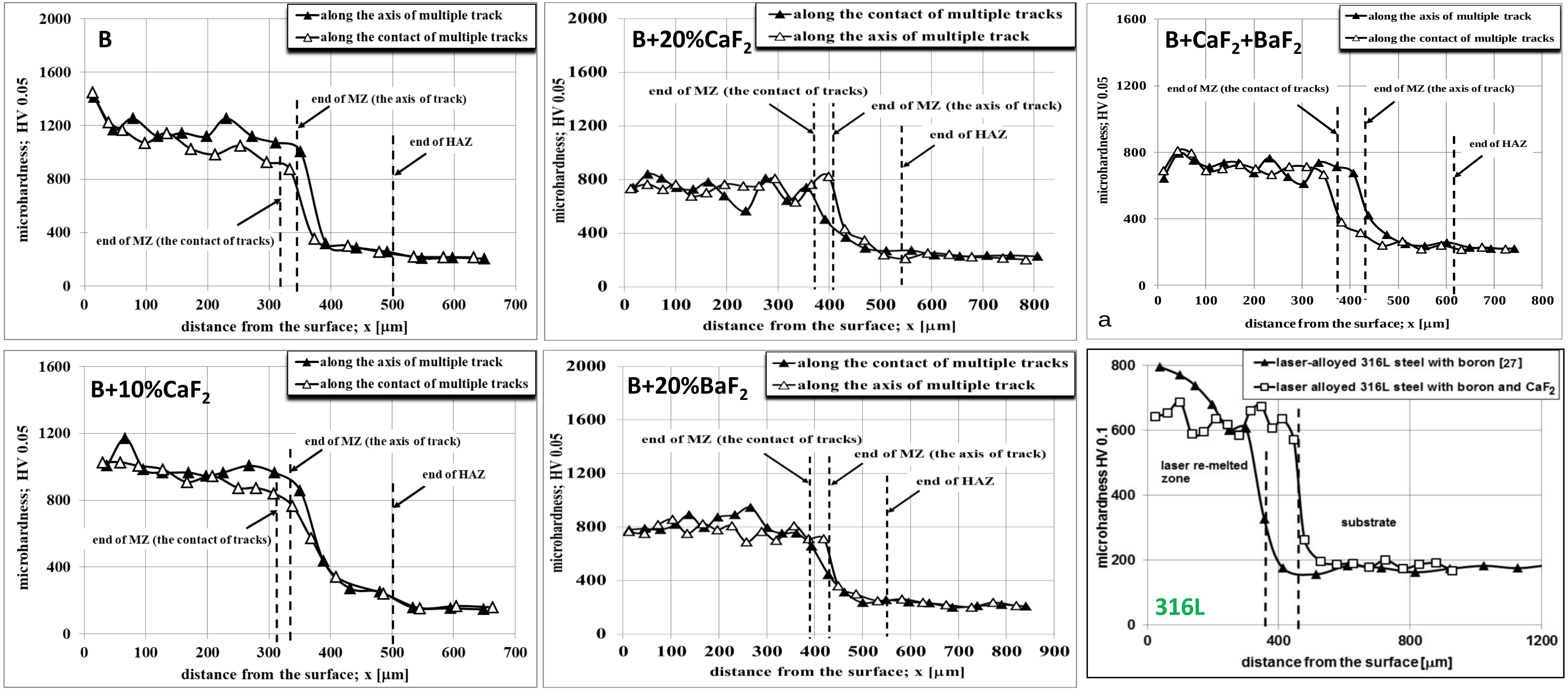

Microhardness profiles of laser-alloyed 100CrMnSi6-4 and 316L steels

Piasecki A., Kulka, M., Kotkowiak, M., Wear resistance improvement of 100CrMnSi6-4 bearing steel by laser boriding using CaF_2 self-lubricating addition, Tribology International, vol. 97, 2016, s. 173-191.
Piasecki A., Kotkowiak M., Kulka M., Self-lubricating surface layers produced using laser alloying of bearing steel, Wear, 2017, 376-377, pp. 993-1008.
Mikołajczak D., **Piasecki A.**, Kulka M., Makuch N., Laser alloying of 316L steel with boron using CaF_2 self-lubricating addition, Inżynieria Materiałowa Materials Engineering, 1 (209), 2016, s.4-9.
Piasecki A., Kotkowiak M., Kulka M., The effect of CaF_2 and BaF_2 solid lubricants on wear resistance of laser-borided 100CrMnSi6-4 bearing steel, Archives of Materials Science and Engineering, 2017, 86(1), pp. 15-23.
Piasecki A., Kotkowiak M., Makuch N., Kulka M., Wear behavior of self-lubricating boride layers produced on Inconel 600-alloy by laser alloying, Wear, 2019, 426-427, pp. 919-933.

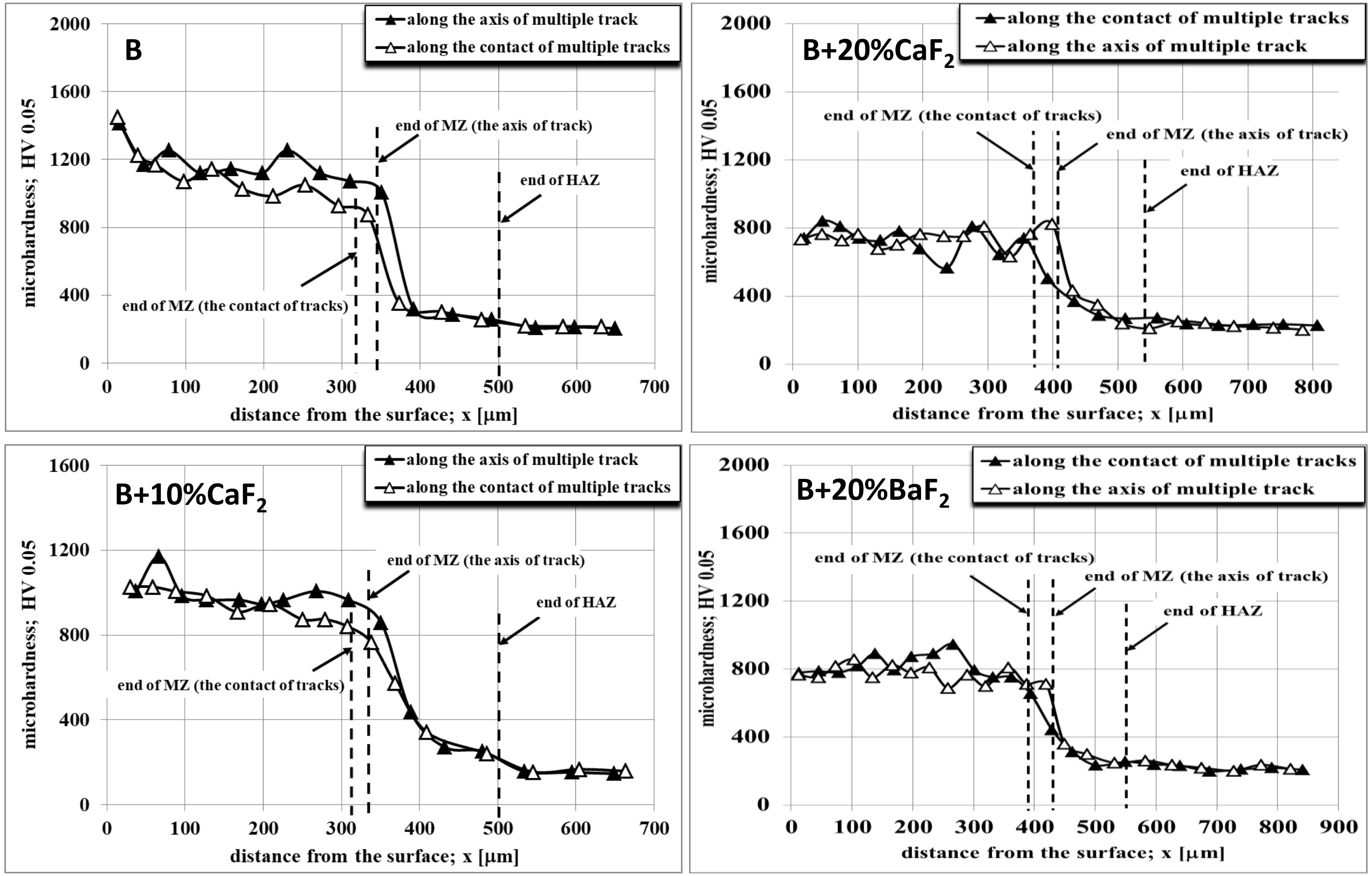

Microhardness profiles of laser-alloyed 100CrMnSi6-4 steel

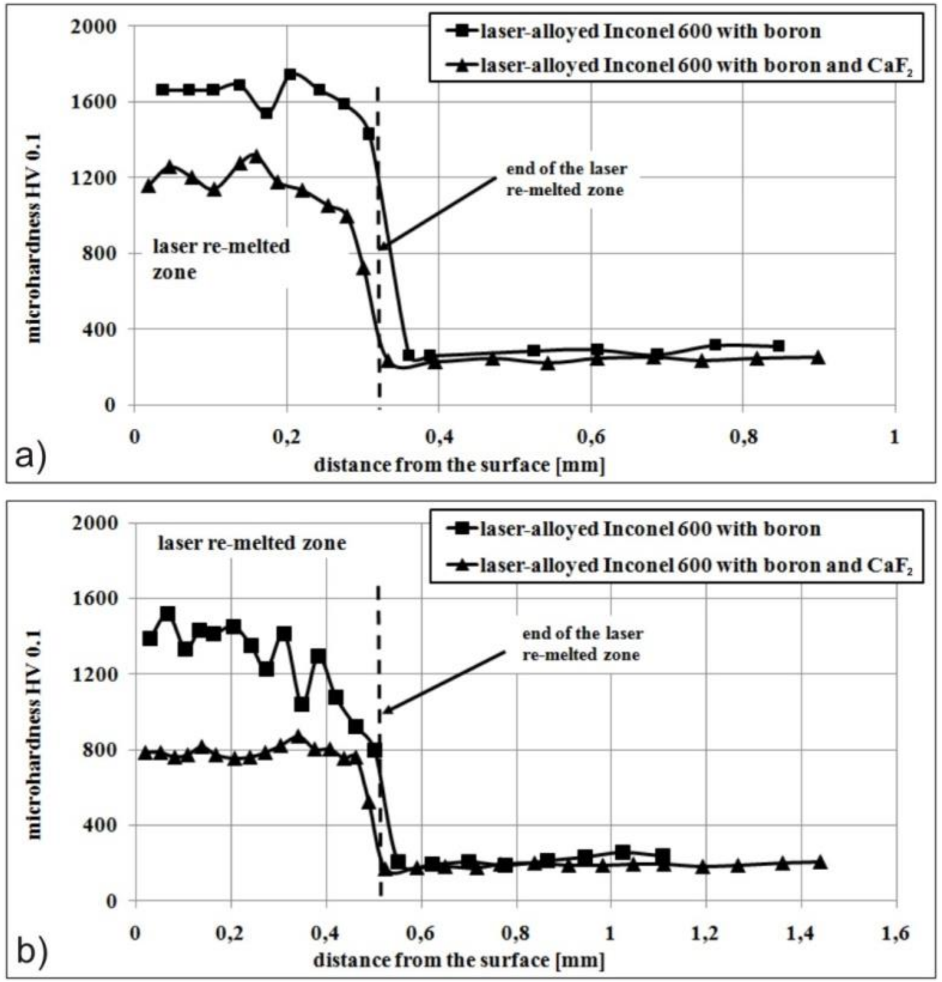

Microhardness profiles of laser-alloyed layers with boron only and laser-alloyed layers with boron and CaF_2, produced at 1.56 kW (a) and 1.95 kW (b).)

Piasecki A., Kulka, M., Kotkowiak, M., Wear resistance improvement of 100CrMnSi6-4 bearing steel by laser boriding using CaF_2 self-lubricating addition, Tribology International, vol. 97, 2016, s. 173-191.
Piasecki A., Kotkowiak M., Kulka M., Self-lubricating surface layers produced using laser alloying of bearing steel, Wear, 2017, 376-377, pp. 993-1008.
Mikołajczak D., **Piasecki A.**, Kulka M., Makuch N., Laser alloying of 316L steel with boron using CaF_2 self-lubricating addition, Inżynieria Materiałowa Materials Engineering, 1 (209), 2016, s.4-9.
Piasecki A., Kotkowiak M., Kulka M., The effect of CaF_2 and BaF_2 solid lubricants on wear resistance of laser-borided 100CrMnSi6-4 bearing steel, Archives of Materials Science and Engineering, 2017, 86(1), pp. 15-23.
Piasecki A., Kotkowiak M., Makuch N., Kulka M., Wear behavior of self-lubricating boride layers produced on Inconel 600-alloy by laser alloying, Wear, 2019, 426-427, pp. 919-933.

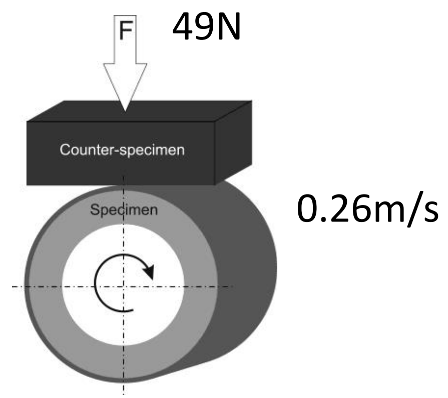

Scheme of the wear test

Chemical composition of sintered carbide S20 [wt %]

Material	WC	(TiC + TaC + NbC)	Co
S20	78	14	8

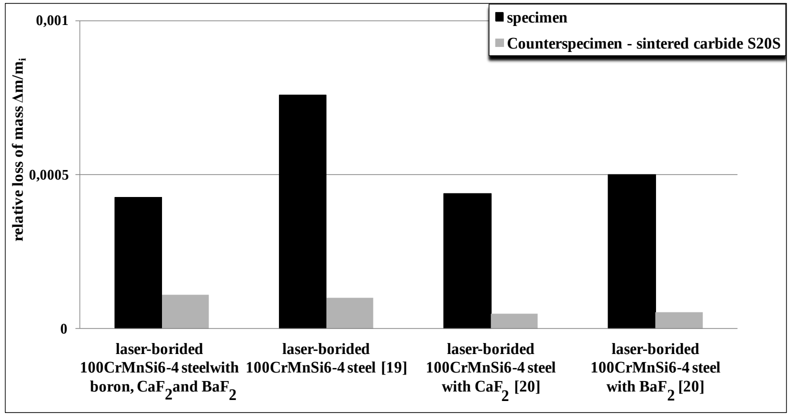

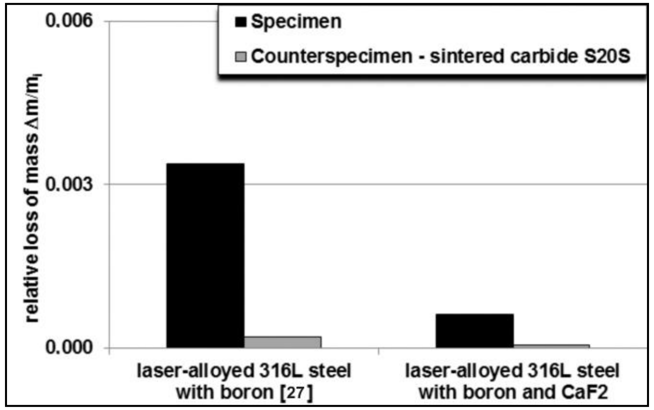

Results of wear tests; relative mass loss of specimens and counter-specimens after two-hour wear test (load F=49N).

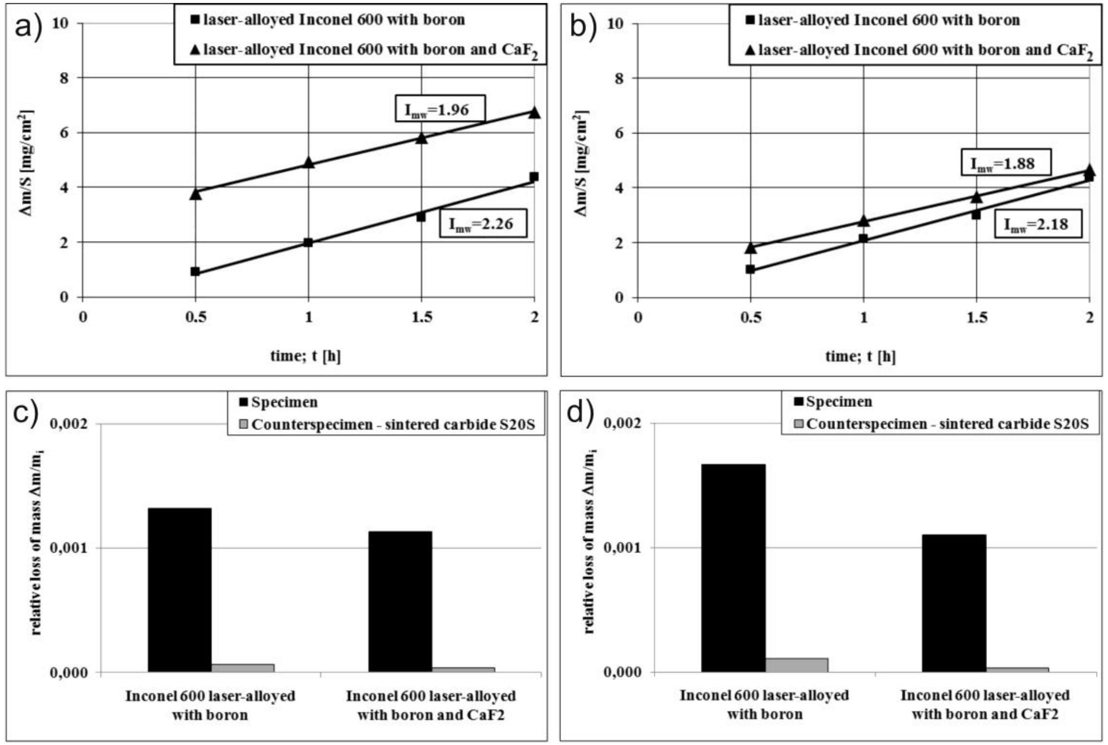

Results of wear tests of laser-alloyed layers with boron only and laser-alloyed layer with boron and CaF_2 at laser beam power of 1.56 kW (a, c) and 1.95 kW (b, d).

Piasecki A., Kulka, M., Kotkowiak, M., Wear resistance improvement of 100CrMnSi6-4 bearing steel by laser boriding using CaF_2 self-lubricating addition, Tribology International, vol. 97, 2016, s. 173-191.
Piasecki A., Kotkowiak M., Kulka M., Self-lubricating surface layers produced using laser alloying of bearing steel, Wear, 2017, 376-377, pp. 993-1008.
Mikołajczak D., **Piasecki A.**, Kulka M., Makuch N., Laser alloying of 316L steel with boron using CaF_2 self-lubricating addition, Inżynieria Materiałowa Materials Engineering, 1 (209), 2016, s.4-9.
Piasecki A., Kotkowiak M., Kulka M., The effect of CaF_2 and BaF_2 solid lubricants on wear resistance of laser-borided 100CrMnSi6-4 bearing steel, Archives of Materials Science and Engineering, 2017, 86(1), pp. 15-23.
Piasecki A., Kotkowiak M., Makuch N., Kulka M., Wear behavior of self-lubricating boride layers produced on Inconel 600-alloy by laser alloying, Wear, 2019, 426-427, pp. 919-933.

Self-lubricating surface layers and composite materials produced by laser alloying and powder metallurgy

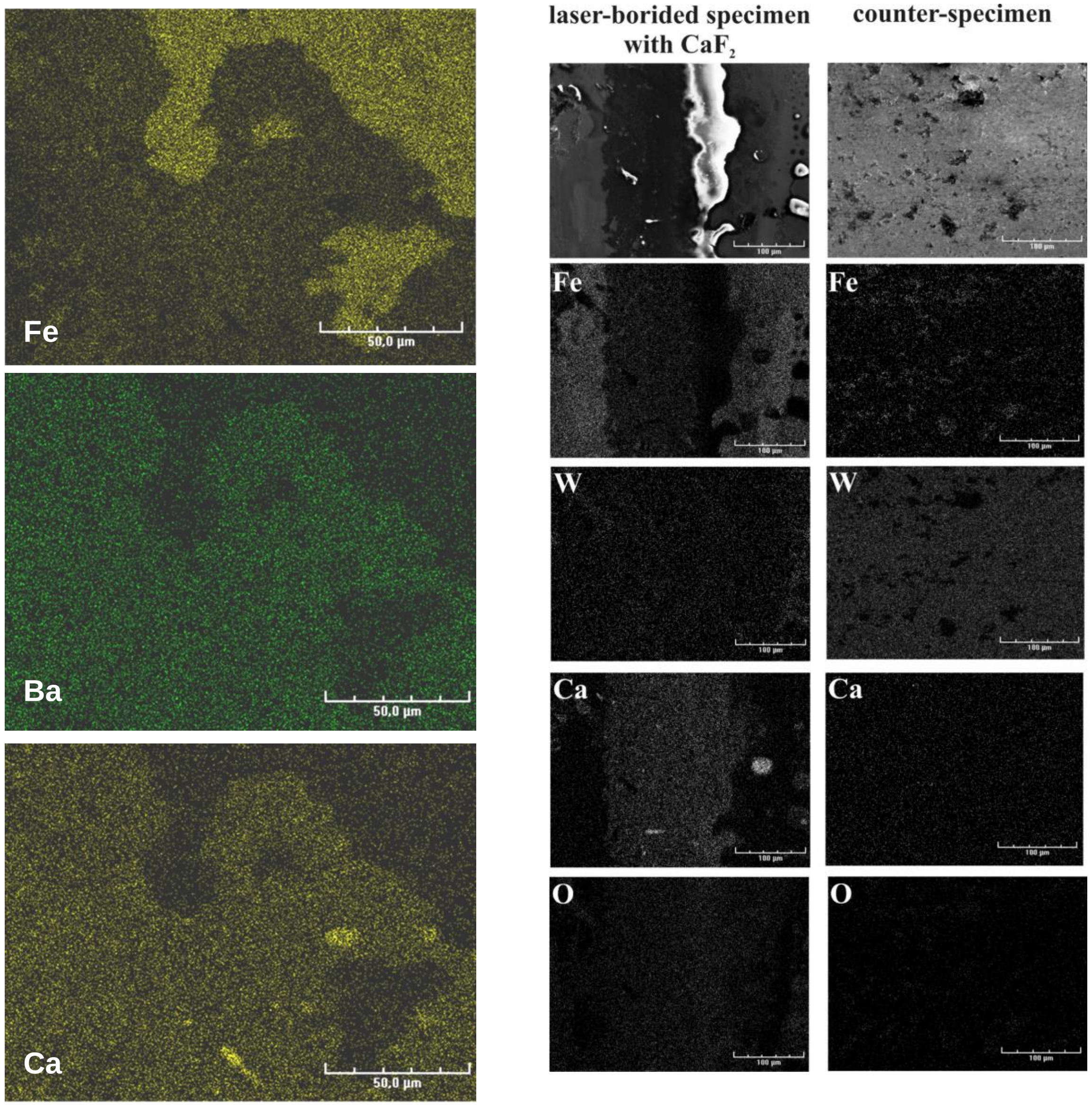

EDS patterns of worn surfaces of laser-alloyed 100CrMnSi6-4 steel with boron, CaF_2, and BaF_2.

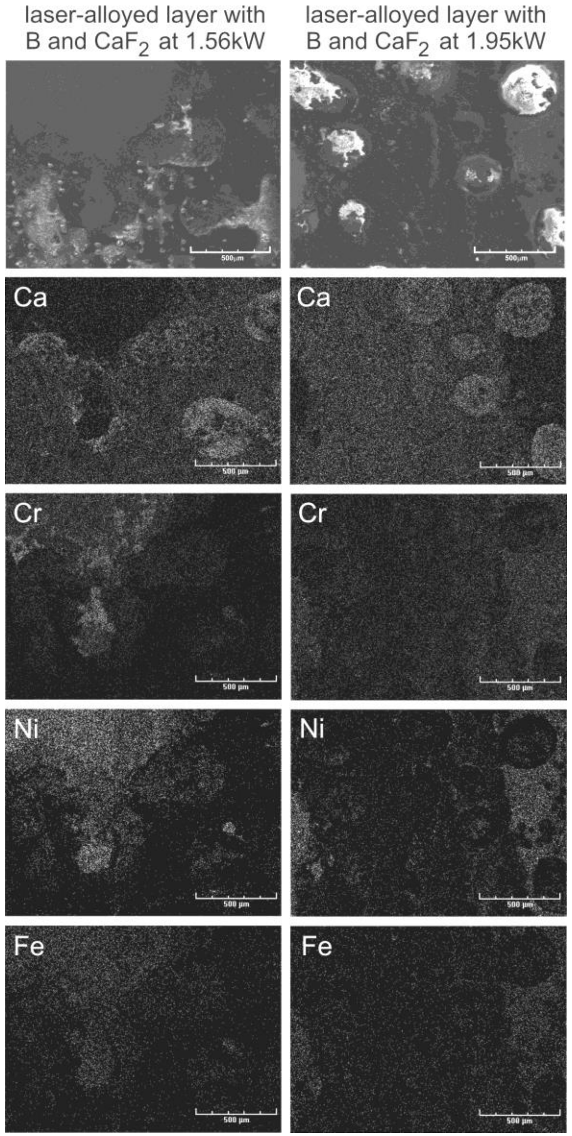

Worn surfaces of laser-alloyed Inconel®600 with boron and CaF_2. EDS patterns of calcium, chromium, nickel and iron.

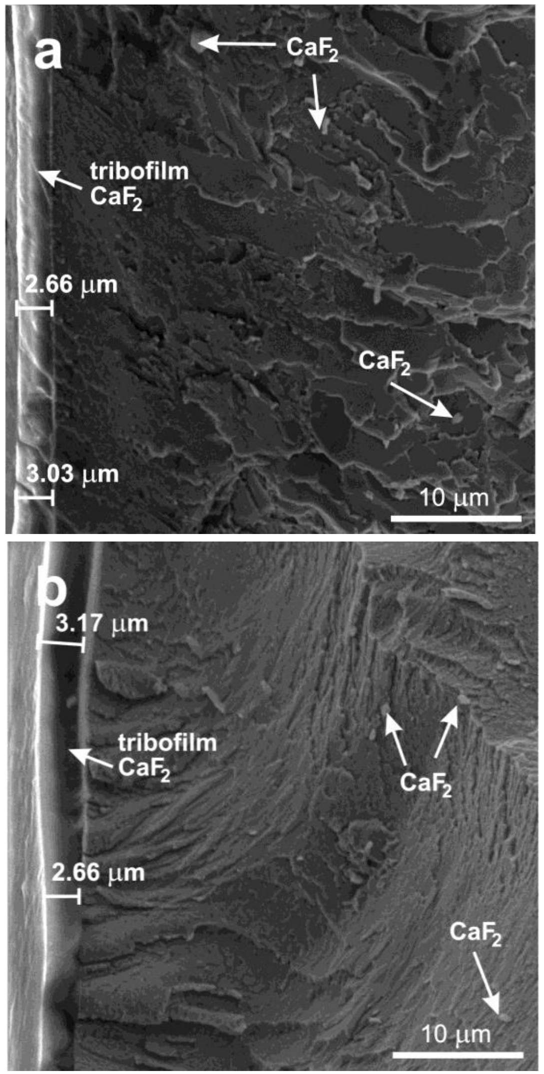

The thickness of tribofilm; laser-alloyed Inconel 600-alloy with boron and CaF_2 at laser beam power of 1.56 kW (a) and 1.95 kW (b).

Piasecki A., Kulka, M., Kotkowiak, M., Wear resistance improvement of 100CrMnSi6-4 bearing steel by laser boriding using CaF_2 self-lubricating addition, Tribology International, vol. 97, 2016, s. 173-191.
Piasecki A., Kotkowiak M., Makuch N., Kulka M., Wear behavior of self-lubricating boride layers produced on Inconel 600-alloy by laser alloying, Wear, 2019, 426-427, pp. 919-933.

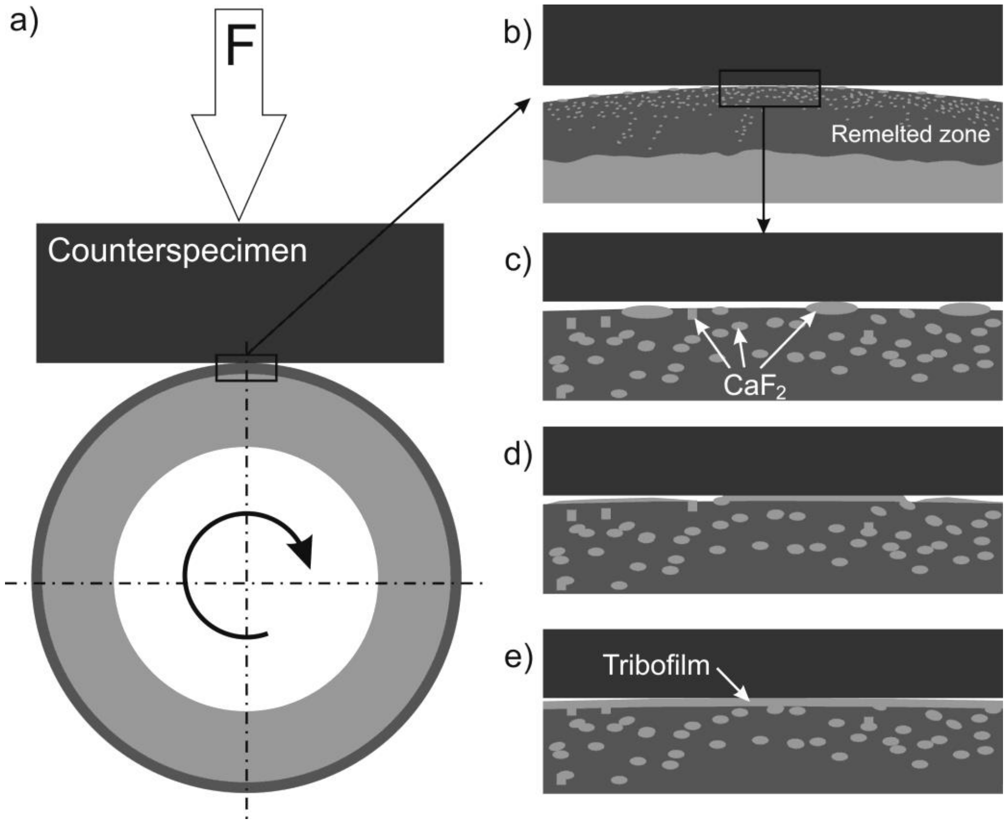

Scheme of tribofilm formation: scheme of the wear test (a), initial stage consisting in grinding-in (b,c), uncovering the lubricant particles and smearing the lubricant on the surface of specimen (d), formation of tribolfilm of diversified thickness (e).

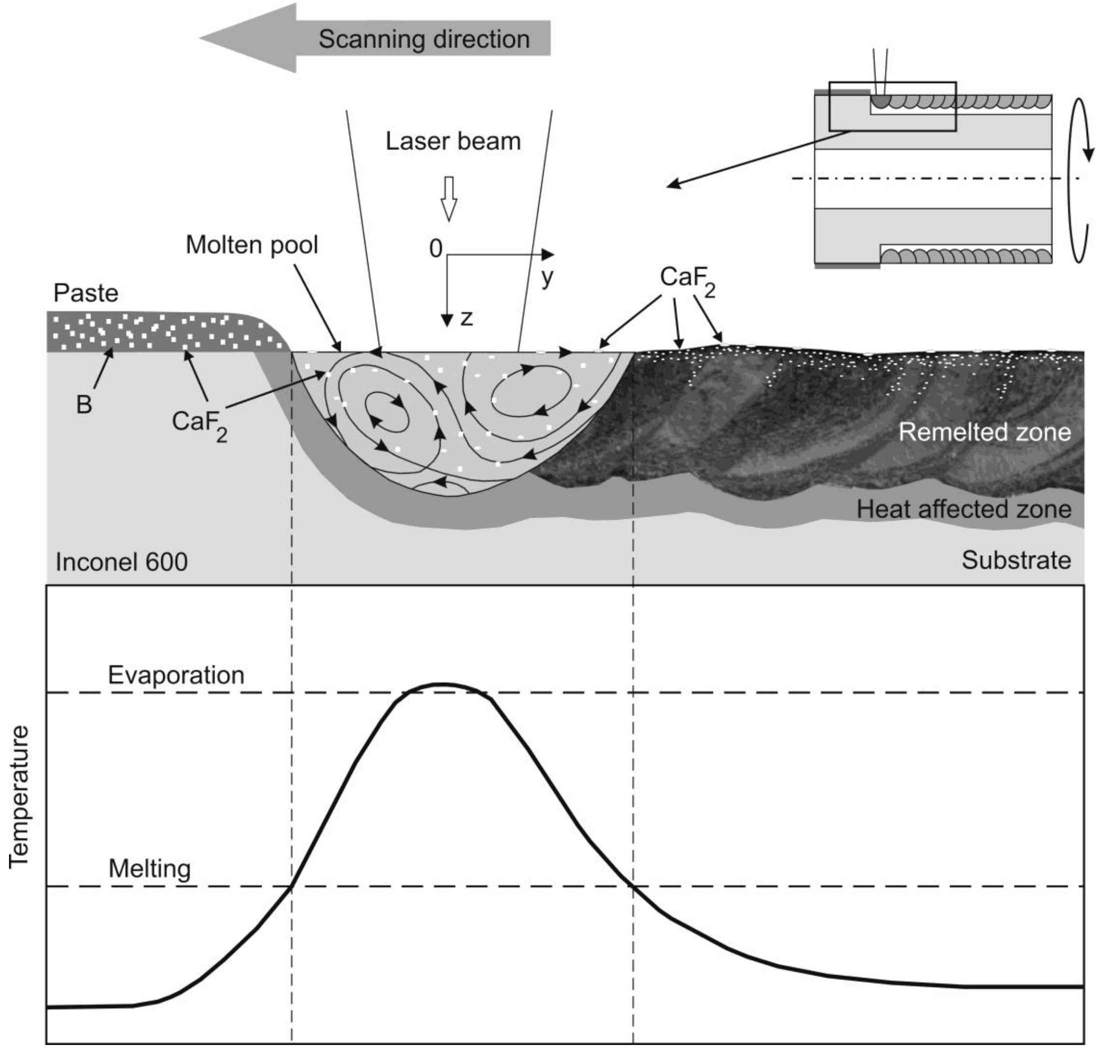

Scheme of the two-stage process of laser alloying of Inconel®600 with boron and CaF_2

Piasecki A., Kulka, M., Kotkowiak, M., Wear resistance improvement of 100CrMnSi6-4 bearing steel by laser boriding using CaF_2 self-lubricating addition, Tribology International, vol. 97, 2016, s. 173-191.
Piasecki A., Kotkowiak M., Kulka M., Self-lubricating surface layers produced using laser alloying of bearing steel, Wear, 2017, 376-377, pp. 993-1008.
Mikołajczak D., **Piasecki A.**, Kulka M., Makuch N., Laser alloying of 316L steel with boron using CaF_2 self-lubricating addition, Inżynieria Materiałowa Materials Engineering, 1 (209), 2016, s.4-9.
Piasecki A., Kotkowiak M., Makuch N., Kulka M., Wear behavior of self-lubricating boride layers produced on Inconel 600-alloy by laser alloying, Wear, 2019, 426-427, pp. 919-933.

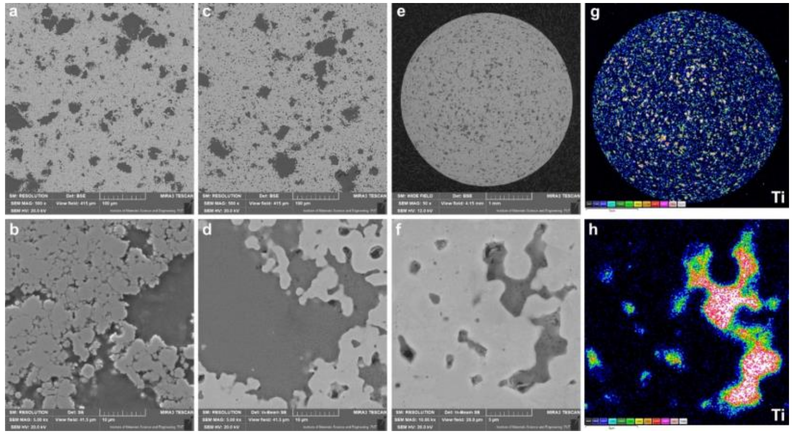

Microstructure of the molding (a,b), sinter (c–f), and EDS distribution map of titanium concentration (g,h).

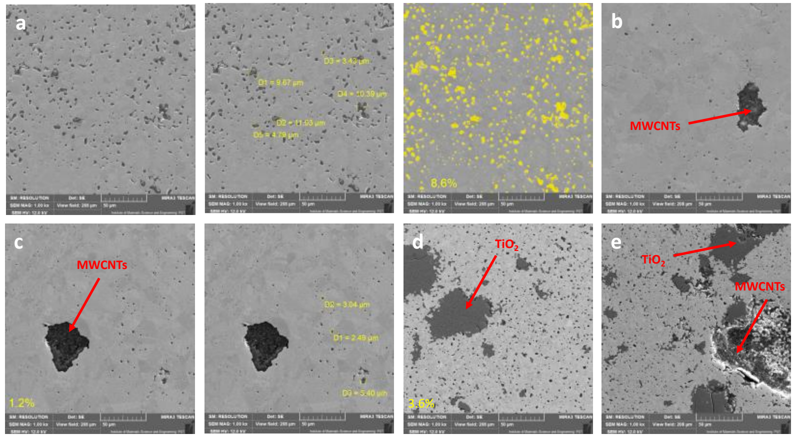

Microstructure of the sinters: Ni (a), Ni+1%MWCNTs (b), Ni+1%MWCNTs-COOH/Ni (c), Ni+1%MWCNTs-5%TiO2 (d), Ni+1%MWCNTs-COOH/Ni+5%TiO2(e).

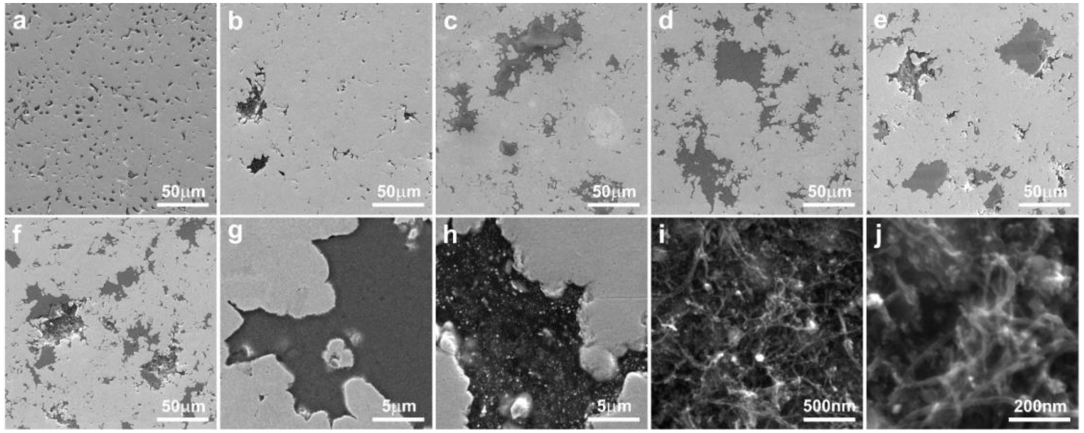

Microstructure of the sinters: Cu (a),Cu-1% CNTs (b,h,i,j), Cu-5% TiO_2 (c), Cu-10% TiO_2 (d,g), Cu-1% CNTs-5% TiO_2 (e), Cu-1% CNTs-10% TiO_2 (f).

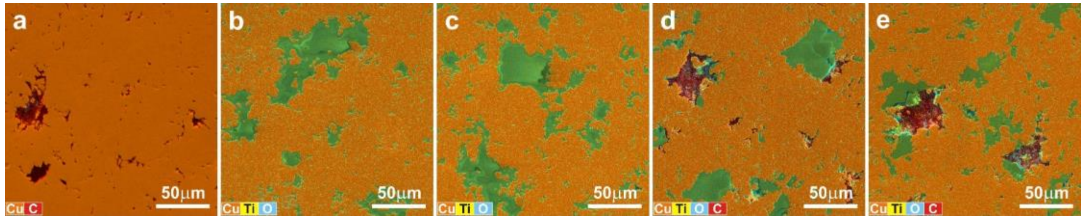

EDS layered image: Cu-1% CNTs (b,h,i,j), Cu-5% TiO_2 (c), Cu-10% TiO_2 (d,g), Cu-1% CNTs-5% TiO_2 (e), Cu-1% CNTs-10% TiO_2 (f).

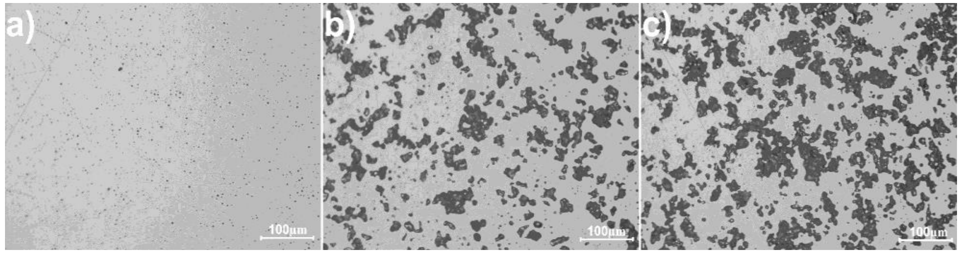

Microstructure of pure Ni sinter (a) and self-lubricating composite: Ni-10%CaF_2 (b) oraz Ni-20%CaF_2 (c).

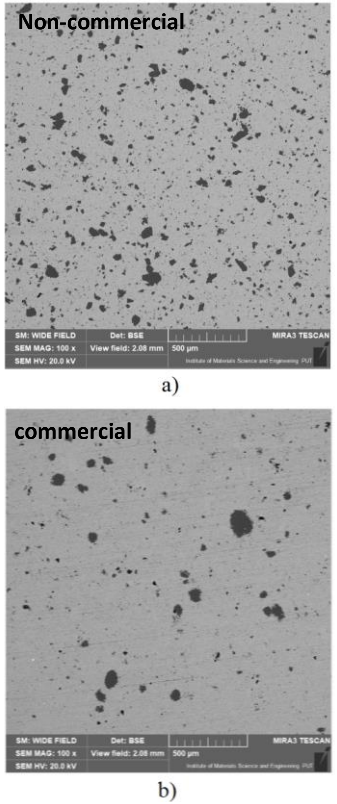

Microstructure of sinters produced by SPS method; Ni + 5% TiO_2, b) Ni + 5% TiO_2. SPS

Piasecki A., Paczos P., Tuliński M., Kotkowiak M., Popławski M., Jakubowicz M., Boncel S., Marek A.A., Buchwald T., Gapiński B., Terzyk A.P., Korczeniewski E., Wieczorowski M., Microstructure, mechanical properties and tribological behavior of Cu-nano TiO_2-MWCNTs composite sintered materials. Wear 2023, vol. 522, s. 204834-1-204834-16

Piasecki A., Kotkowiak M., Tulinski, M., Čep R. Tribological Properties of Cu-MoS_2-WS_2-Ag-CNT Sintered Composite Materials. Materials 2022, 15, 8424.

Piasecki A., Kotkowiak M., Tulinski M., Kubiak A. Tribological Behavior and Wear Mechanism of Ni-Nano TiO_2 Composite Sintered Material at Room Temperature and 600 °C. Lubricants 2022, 10, 120.

Kotkowiak M., **Piasecki A.**, Kulka M., The influence of solid lubricant on tribological properties of sintered Ni–20%CaF2 composite material, Ceramics International, 2019, 45(14), pp. 17103-17113.

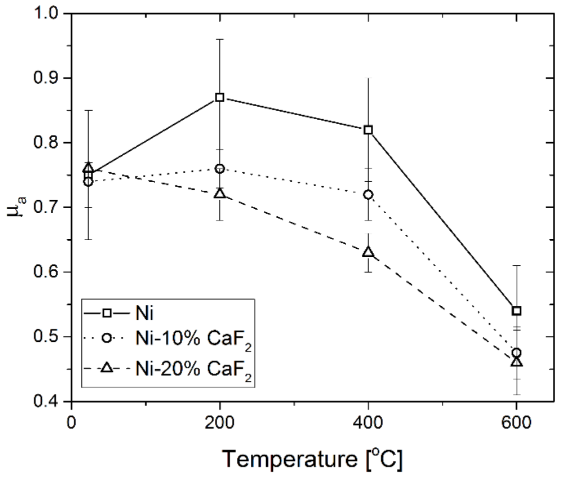

The average values of the friction coefficient vs. temperature of friction for pure Ni, sintered Ni-10% CaF_2 and sintered Ni-20% CaF_2 self-lubricating composites mating with Inconel®625-alloy.

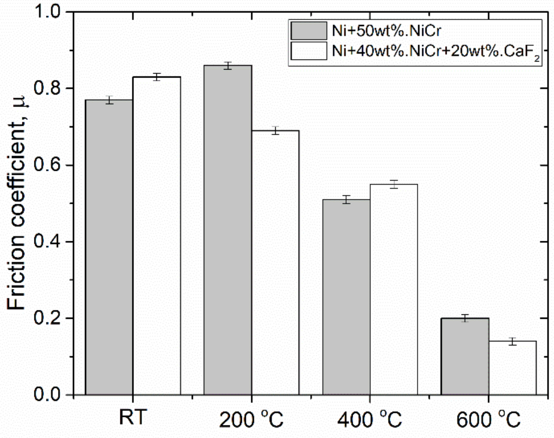

The average values of the friction coefficient vs. temperature of friction for sintered self-lubricating composites mating with Inconel®625-alloy.

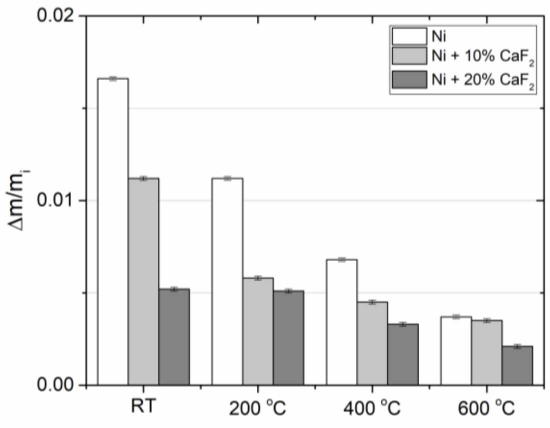

Relative loss of mass of the counter-samples.

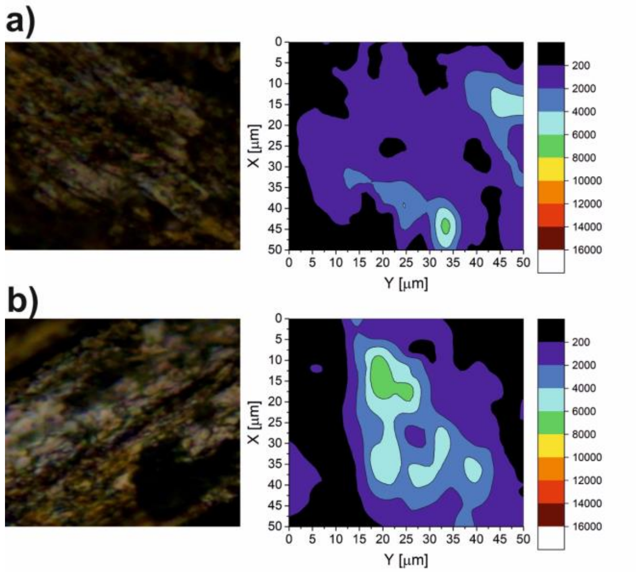

The Raman maps of Ni-10% CaF_2 (a) and Ni-20% CaF_2 (b) self-lubricating composites after wear test at 600°C.

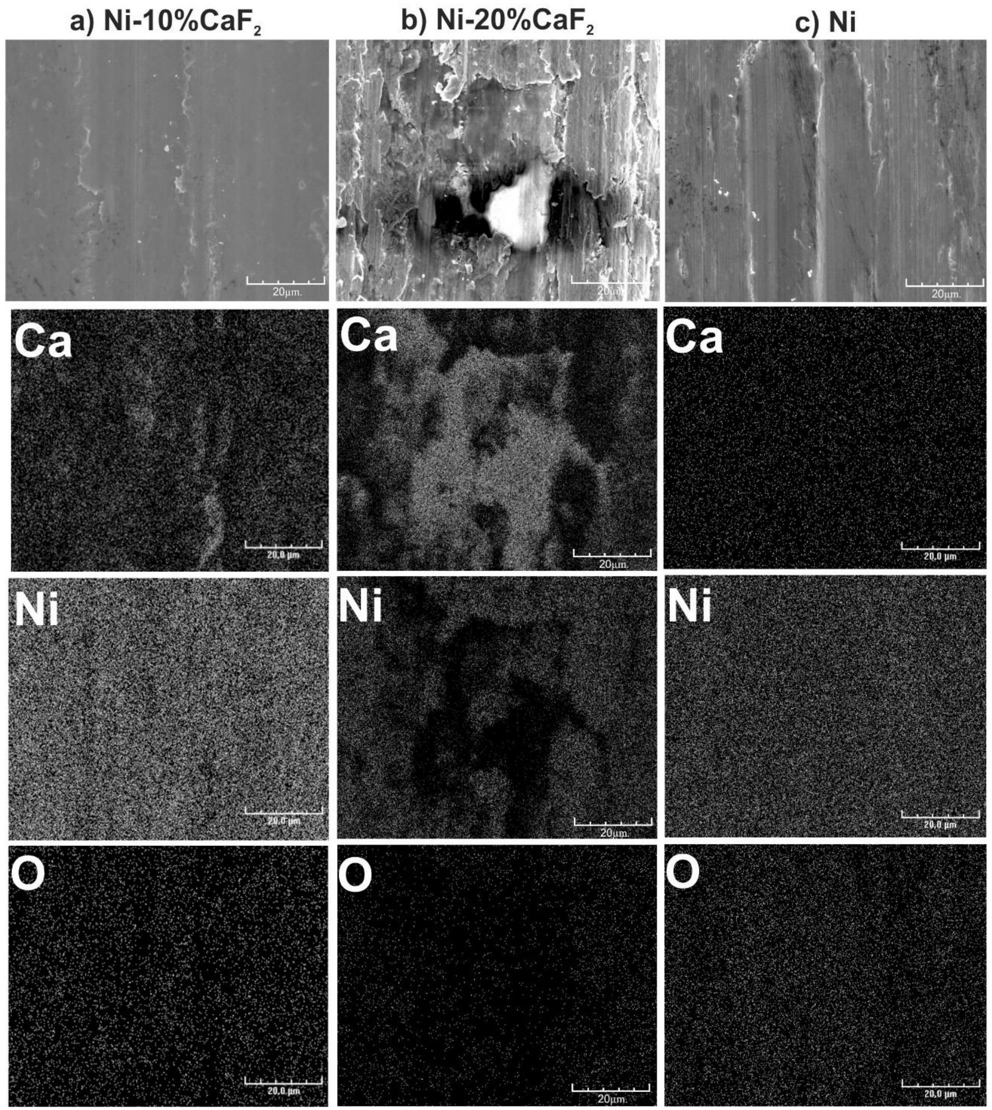

Worn surfaces of sinters after test at 600°C. EDS patterns of calcium, nickel and oxygen.

Kotkowiak M., **Piasecki A.**, Kulka M., The influence of solid lubricant on tribological properties of sintered Ni–20%CaF2 composite material, Ceramics International, 2019, 45(14), pp. 17103-17113.
Kotkowiak M., **Piasecki A.**, M. Kotkowiak, T. Buchwald, The Mechanism of Wear Reduction in the Ni-CaF2 Composite Material: Raman and Confocal Microscopy Insights, Materials 2022, 15, 5501.
Kotkowiak M., **Piasecki A.**, Characterization of Wear Properties of Pure Nickel Modified by Ni-Cr Composite and CaF2 Solid Lubricant Addition. Materials 2022, 15, 7511.

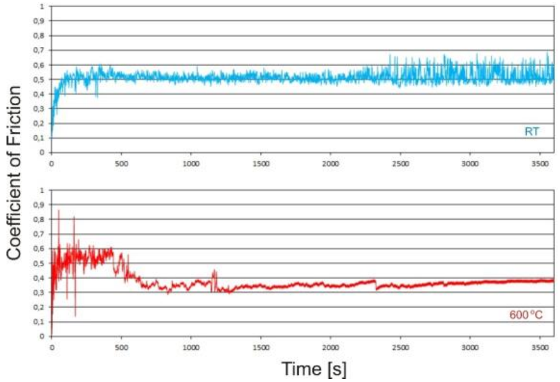

Coefficient of friction vs. time of friction of self-lubricating composite cooperating with Inconel®625-alloy at room temperature and 600°C.

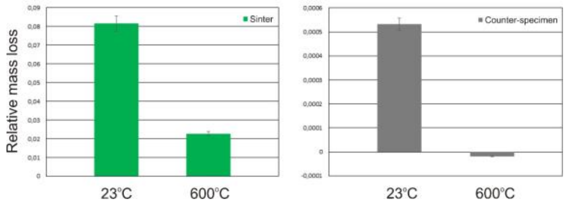

Relative mass loss of sinters and counter-samples at room temperature and 600°C.

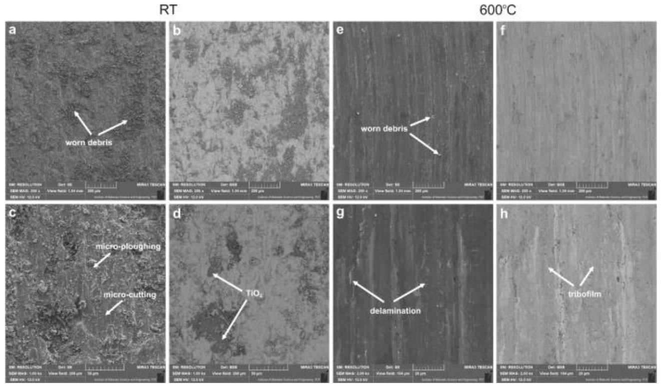

Worn surface of sinters after friction wear tests at 23°C (a–d), and at 600°C (e–h), SEM.

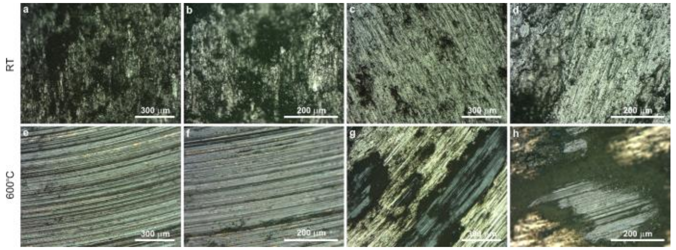

Worn surface of sinters and counter-samples after friction wear tests at 23°C—sinter (a,b), counter-sample (c,d) and at 600°C—sinter (e,f), counter-sample (g,h), LM.

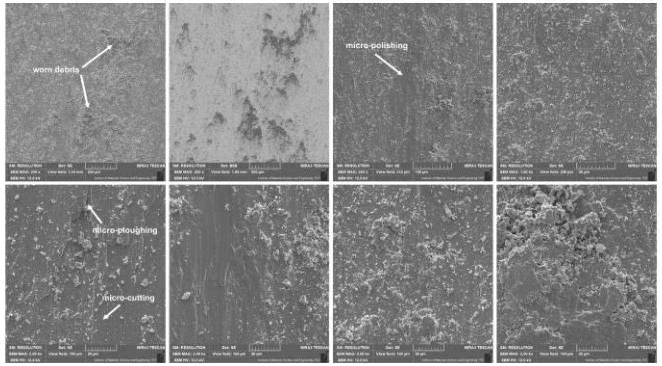

Worn surface of counter-samples after friction wear tests at room temperature, SEM.

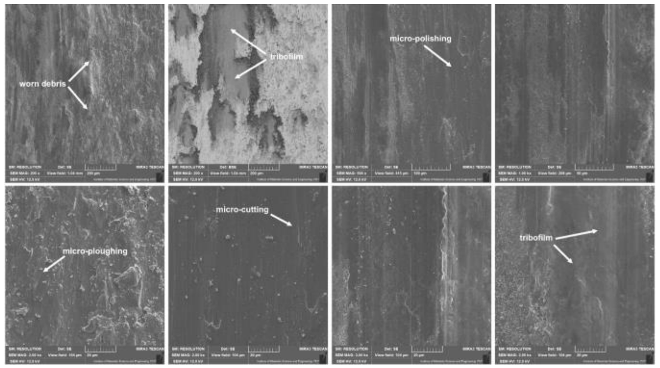

Worn surface of counter-samples after friction wear tests at 600°C, SEM.

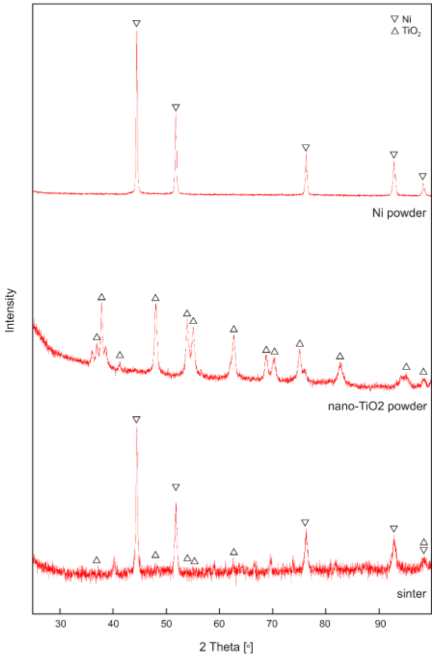

XRD patterns of powders and sinter.

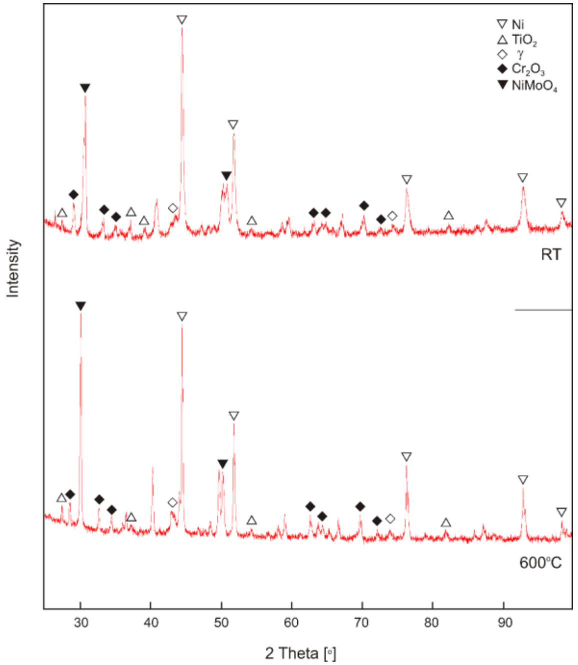

XRD patterns of worn surfaces.

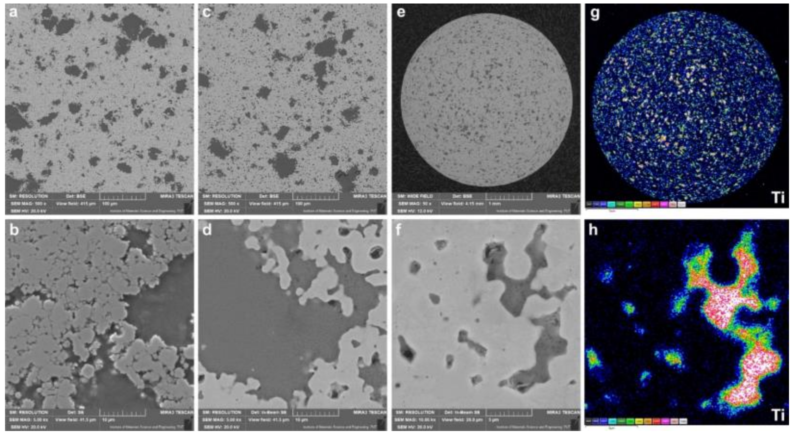

Microstructure of the molding (a,b), sinter (c–f), and EDS distribution map of titanium concentration (g,h).

Piasecki A., Kotkowiak M., Tulinski M., Kubiak A. Tribological Behavior and Wear Mechanism of Ni-Nano TiO2 Composite Sintered Material at Room Temperature and 600 °C. Lubricants 2022, 10, 120.

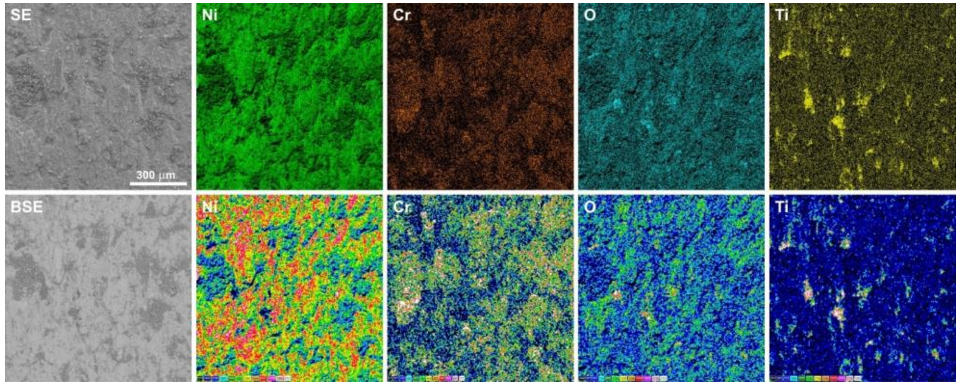

EDS maps of element concentration distributions on the sinter surface after friction wear test at room temperature.

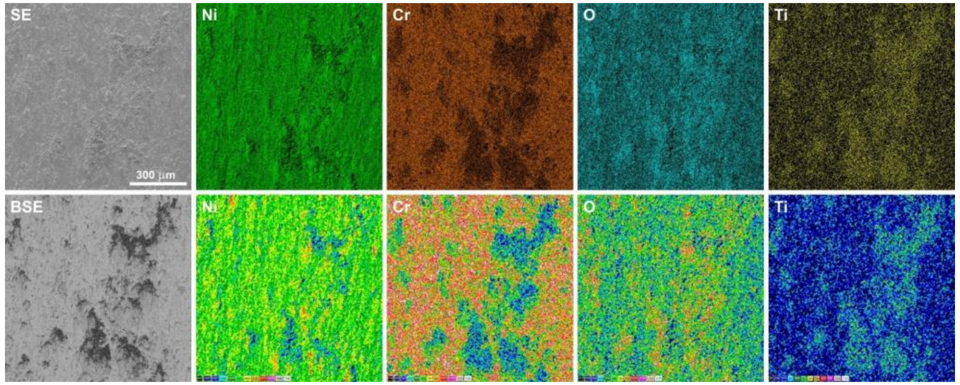

EDS maps of element concentration distributions on the Inconel®625 surface after friction wear test at room temperature.

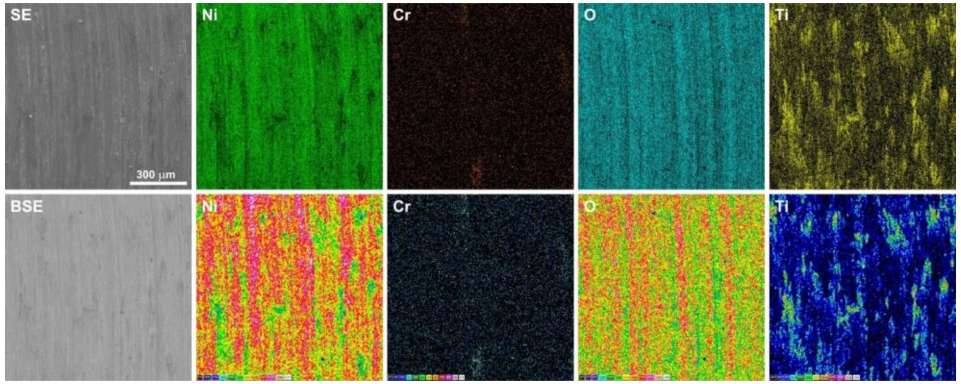

EDS maps of element concentration distributions on the sinter surface after friction wear test at 600°C.

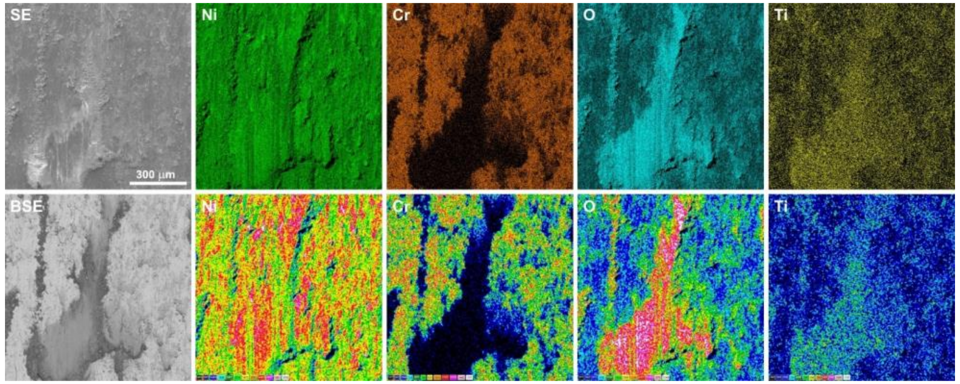

EDS maps of element concentration distributions on the Inconel®625 surface after friction wear test at 600°C.

Piasecki A., Kotkowiak M., Tulinski M., Kubiak A. Tribological Behavior and Wear Mechanism of Ni-Nano TiO2 Composite Sintered Material at Room Temperature and 600 °C. Lubricants 2022, 10, 120.

The chemical composition of powder mixes used in order to produce the sinters.

	Chemical Composition [wt. %]				
No.	Cu	MoS_2	WS_2	Ag	CNTs
1	bal.			10	
2	bal.	20			
3	bal.		20		
4	bal.				2
5	bal.	5	5		
6	bal.	5	5	2	
7	bal.	5	5	2	2
8	bal.	5	5		2

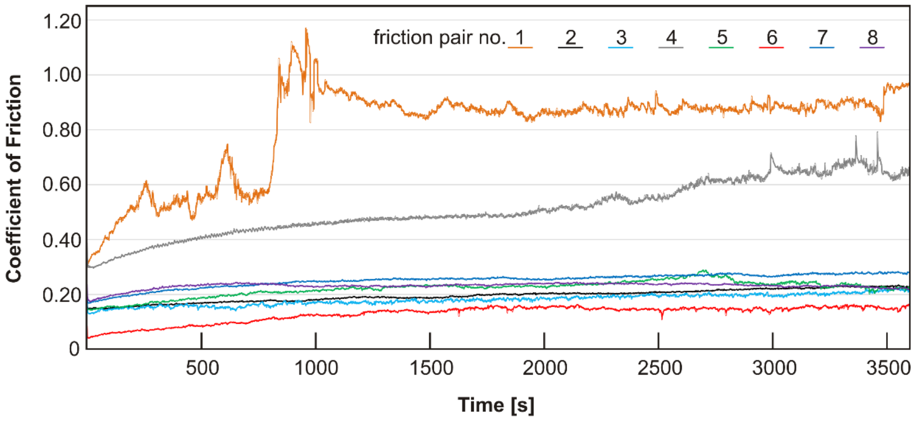

Friction coefficient vs. time of friction self-lubricating composite mating with Inconel®625 alloy at room temperature.

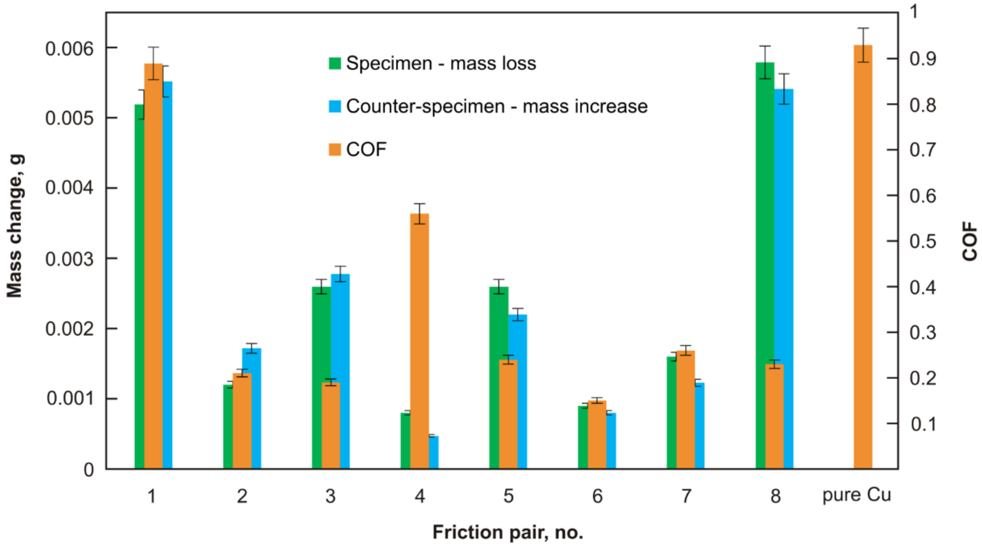

The average friction coefficients and mass changes.

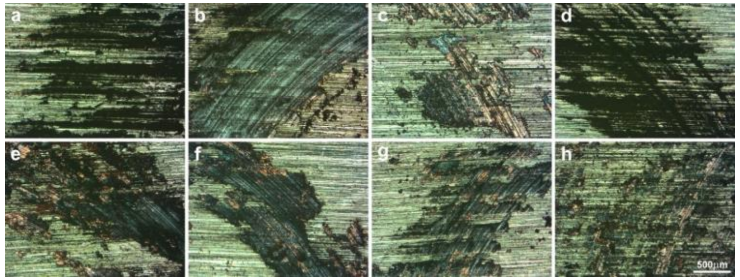

Worn surfaces of the counter-specimens tested at RT (LM); friction pair no.1 (a), 2 (b), 3 (c), 4 (d), 5 (e), 6 (f), 7 (g) i 8 (h).

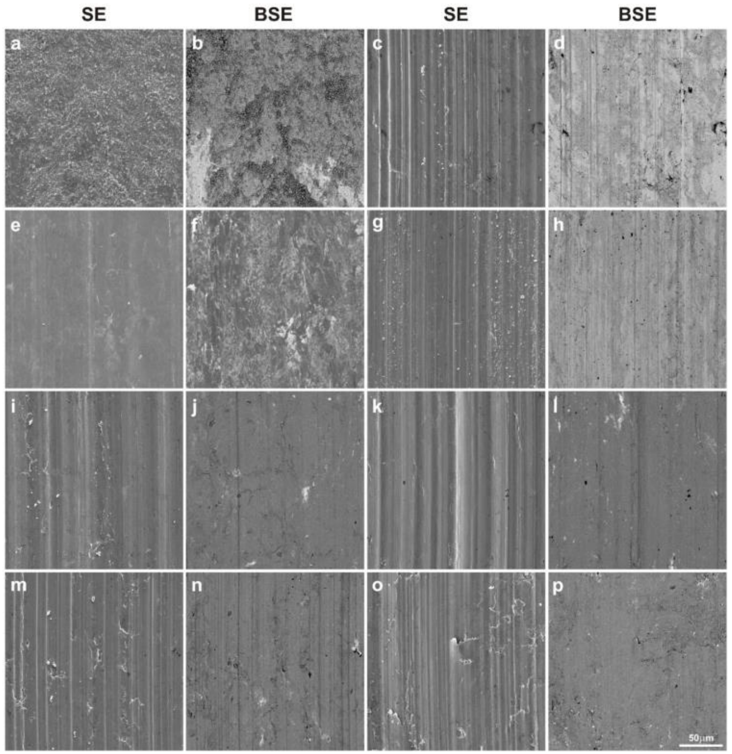

Worn surfaces of the sinters tested at RT (SEM); friction pair no. 1 (a,b), 2 (c,d), 3 (e,f), 4 (g,h), 5 (i,j), 6 (k,l), 7 (m,n) and 8 (o,p).

Piasecki, A., Kotkowiak, M., Tulinski, M., Čep, R. Tribological Properties of Cu-MoS_2-WS_2-Ag-CNT Sintered Composite Materials. Materials 2022, 15, 8424.

1 (Cu-10% Ag), 2 (Cu-20% MoS_2), 3 (Cu-20% WS_2), 4 (Cu-1%CNTs), 5 (Cu-5% MoS_2-5% WS_2), 6 (Cu-5% MoS_2-5% WS_2-2% Ag), 7 (Cu-5% MoS_2-5% WS_2-2% Ag-2%CNTs), 8 (Cu-5% MoS_2-5% WS_2-2% CNTs)

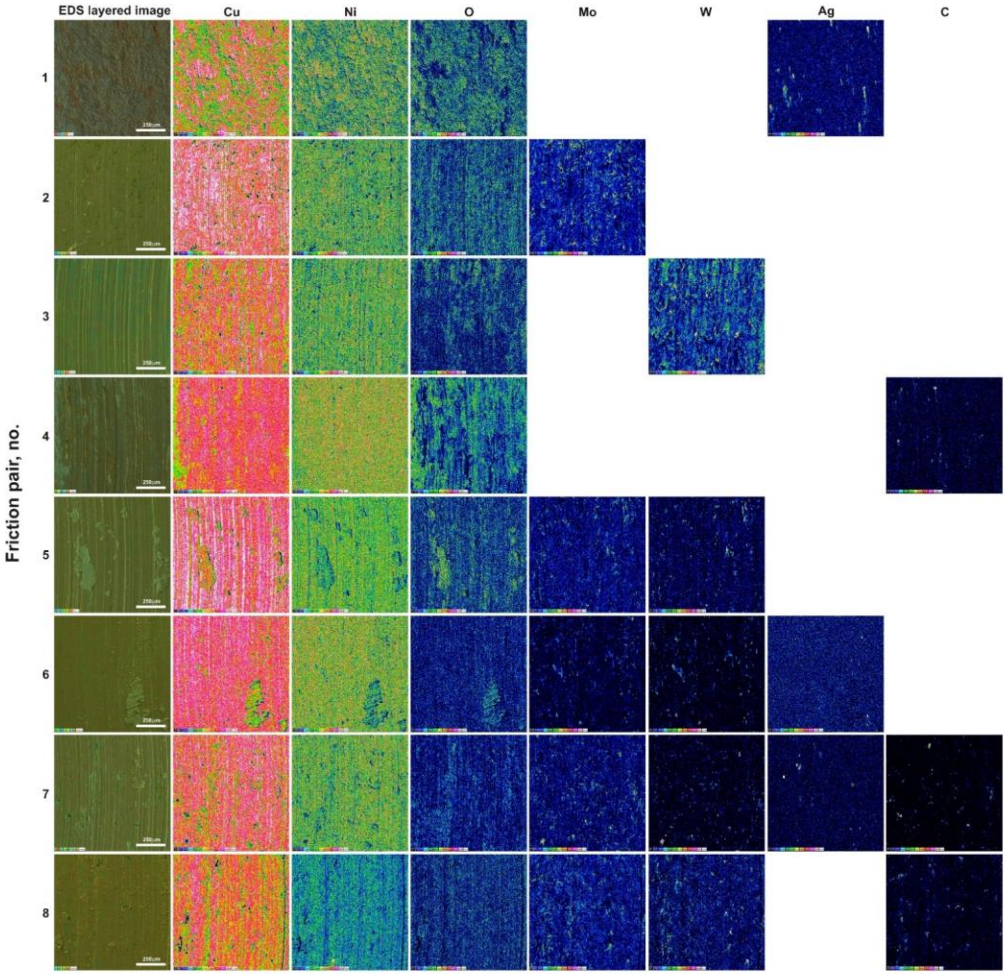

Worn surfaces of the specimens (sintered composite materials) tested at RT (EDS maps).

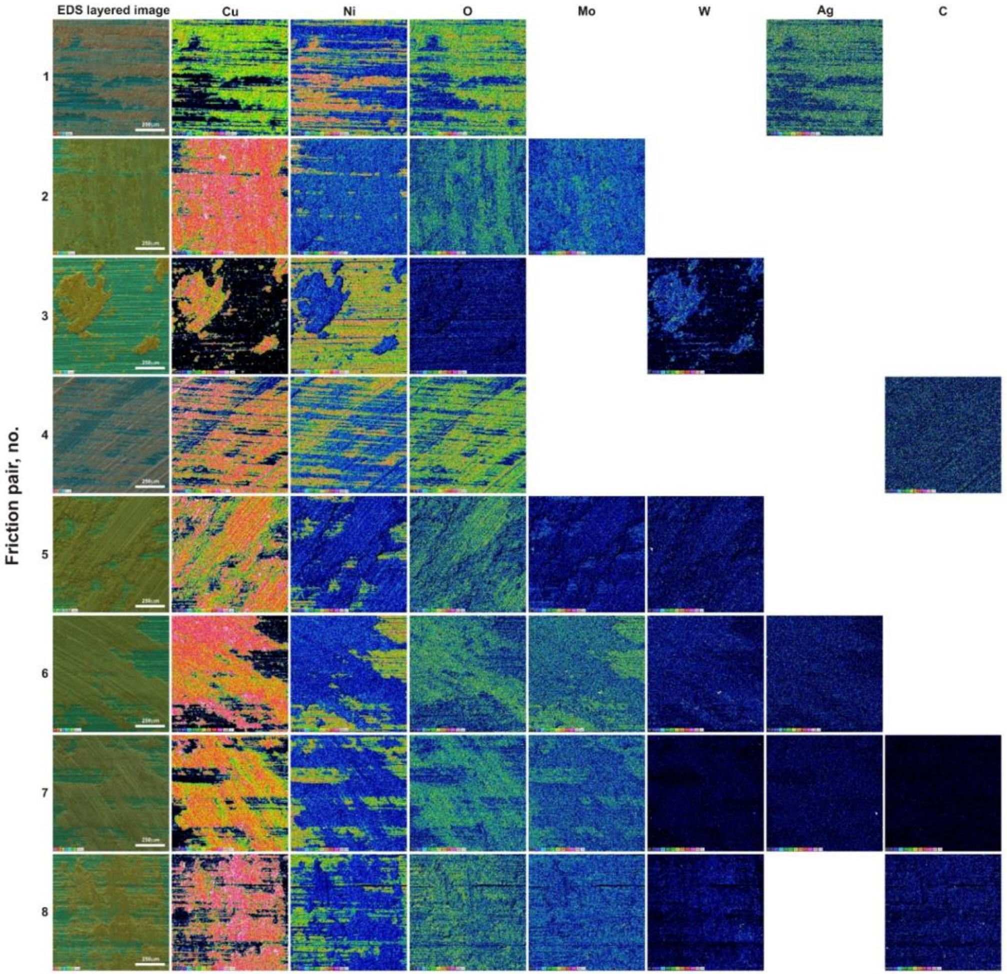

Worn surfaces of the counter-specimens (Inconel®625 alloy) tested at RT (EDS maps).

Piasecki, A., Kotkowiak, M., Tulinski, M., Čep, R. Tribological Properties of Cu-MoS_2-WS_2-Ag-CNT Sintered Composite Materials. Materials 2022, 15, 8424.

The chemical composition of powder and sinters.

Chemical composition [% wt.]			
No.	Cu	CNTs	TiO_2
1	bal.		
2	bal.	1	
3	bal.		5
4	bal.		10
5	bal.	1	5
6	bal.	1	10

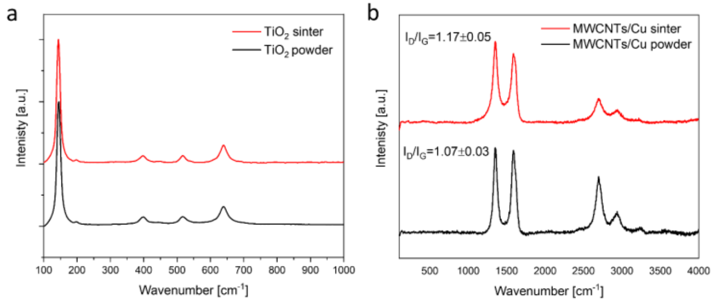

Raman spectra of TiO_2 (a) and CNTs (b).

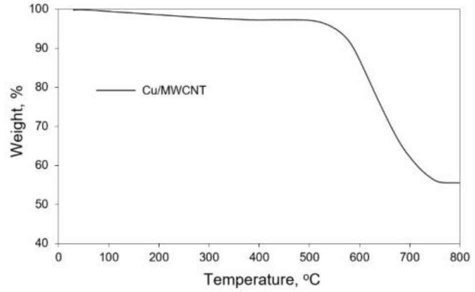

TGA curve of the MWCNTs/Cu hybrid.

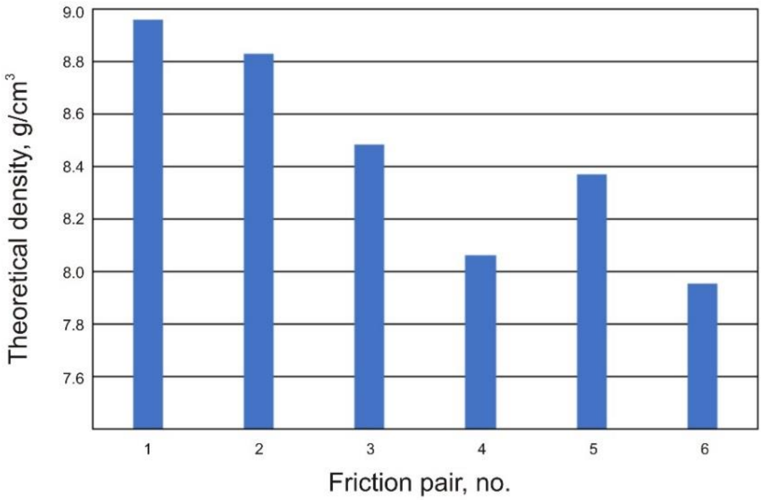

Theoretical densities of the sinters

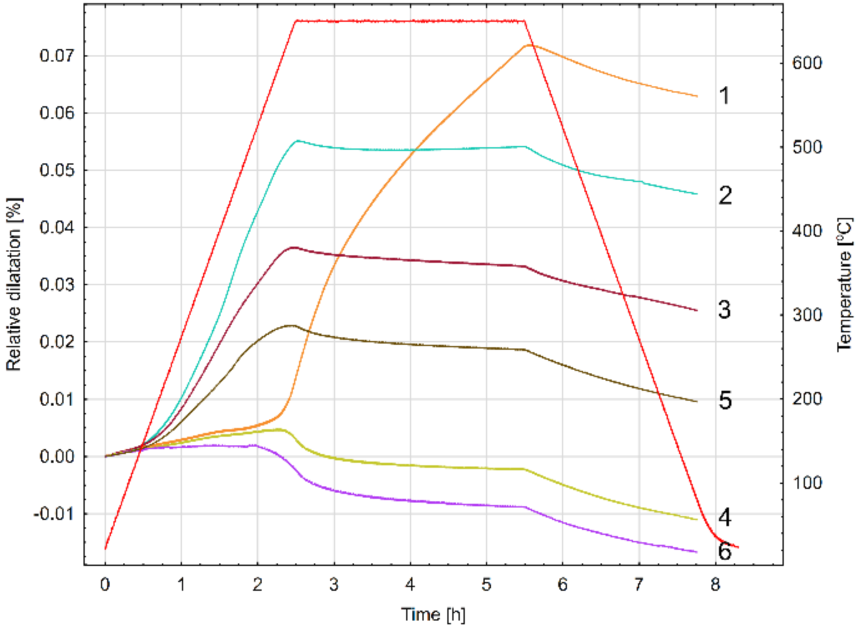

Dilatometric curves and heat treatment scheme of tested samples.

Cu - 8.96 g/cm^3
TiO_2 - 4.23 g/cm^3
MWCNTs - 2.1 g/cm^3
MWCNTs/Cu - 3.66 g/cm^3

Piasecki A., Paczos P., Tuliński M., Kotkowiak M., Popławski M., Jakubowicz M., Boncel S., Marek A.A., Buchwald T., Gapiński B., Terzyk A.P., Korczeniewski E., Wieczorowski M., Microstructure, mechanical properties and tribological behavior of Cu-nano TiO_2-MWCNTs composite sintered materials. Wear 2023, vol. 522, s. 204834-1-204834-16

Results of experimental investigations.

Sinter no.		F_{max} [N]	Average E_{mod} [kN/mm]	W to F_{max} [Nmm]	Average hardness HV5	Chemical composition [% wt.] No.	Cu	MWCNTs	nano-TiO_2
1		8000	5.36	3948	26.35	1	bal.		
2		8000	6.33	4381	36.47	2	bal.	1	
3		8000	**7.60**	4072	**68.24**	3	bal.		5
4		8000	**7.83**	4148	**84.94**	4	bal.		10
5		8000	6.77	**4746**	56.12	5	bal.	1	5
6		8000	7.12	**4762**	61.66	6	bal.	1	10

Test stand and sinter (before and after the compression test).

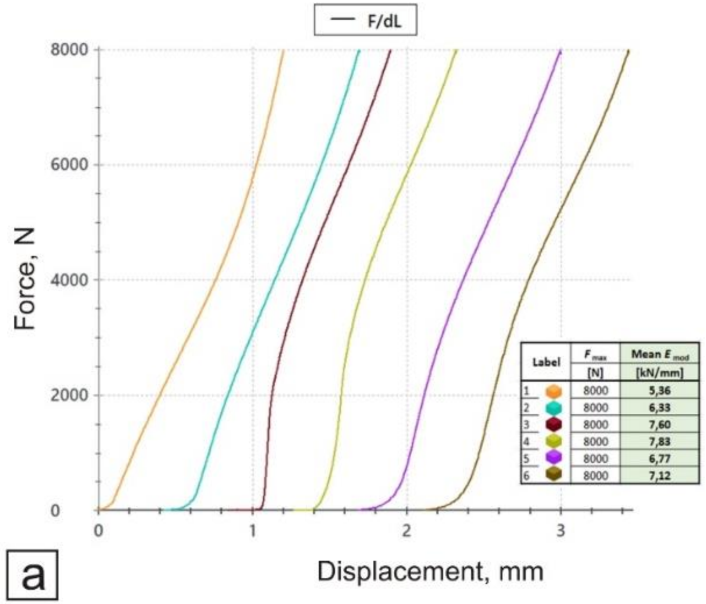

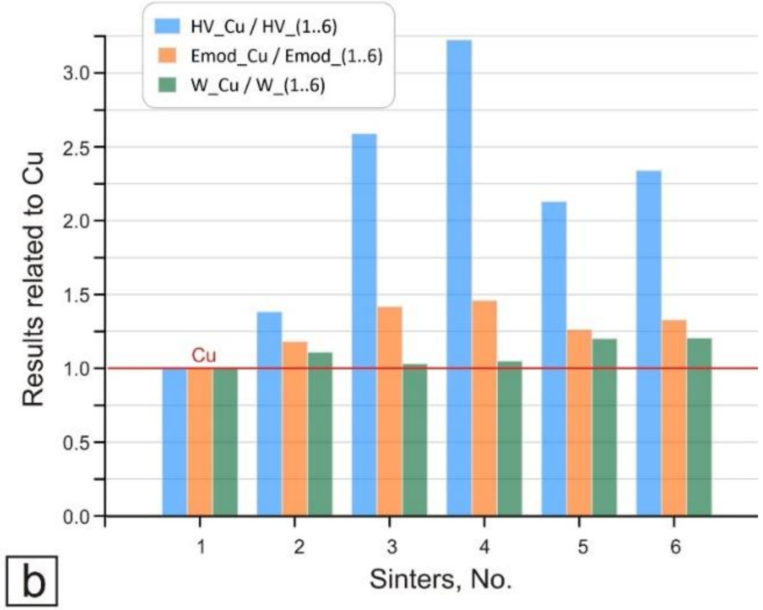

Force-displacement diagram (a); results related to copper (b).

Piasecki A., Paczos P., Tuliński M., Kotkowiak M., Popławski M., Jakubowicz M., Boncel S., Marek A.A., Buchwald T., Gapiński B., Terzyk A.P., Korczeniewski E., Wieczorowski M., Microstructure, mechanical properties and tribological behavior of Cu-nano TiO_2-MWCNTs composite sintered materials. Wear 2023, vol. 522, s. 204834-1-204834-16

1 (Cu), 2 (Cu-1% CNTs), 3 (Cu-5% TiO_2), 4 (Cu-10% TiO_2), 5 (Cu-1% CNTs-5% TiO_2), 6 (Cu-1% CNTs-10% TiO_2)

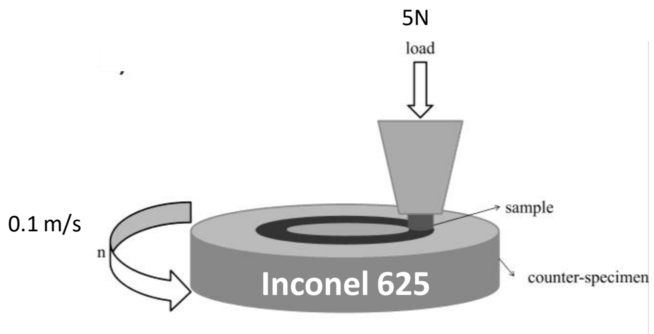

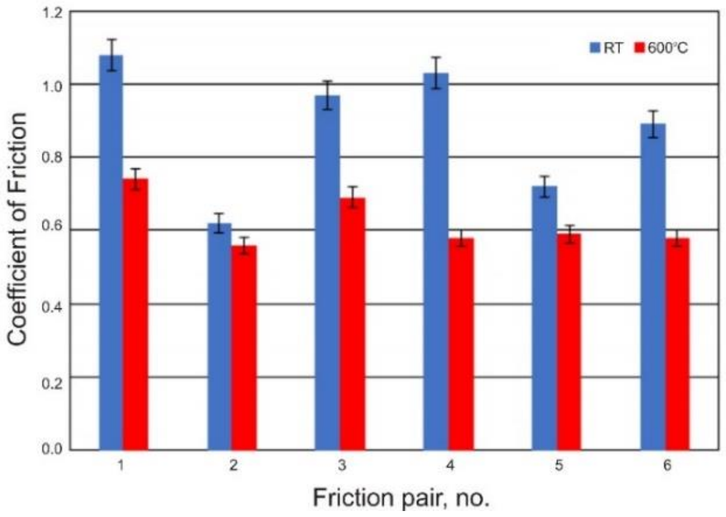

Coefficient of friction at room temperature and 600°C.

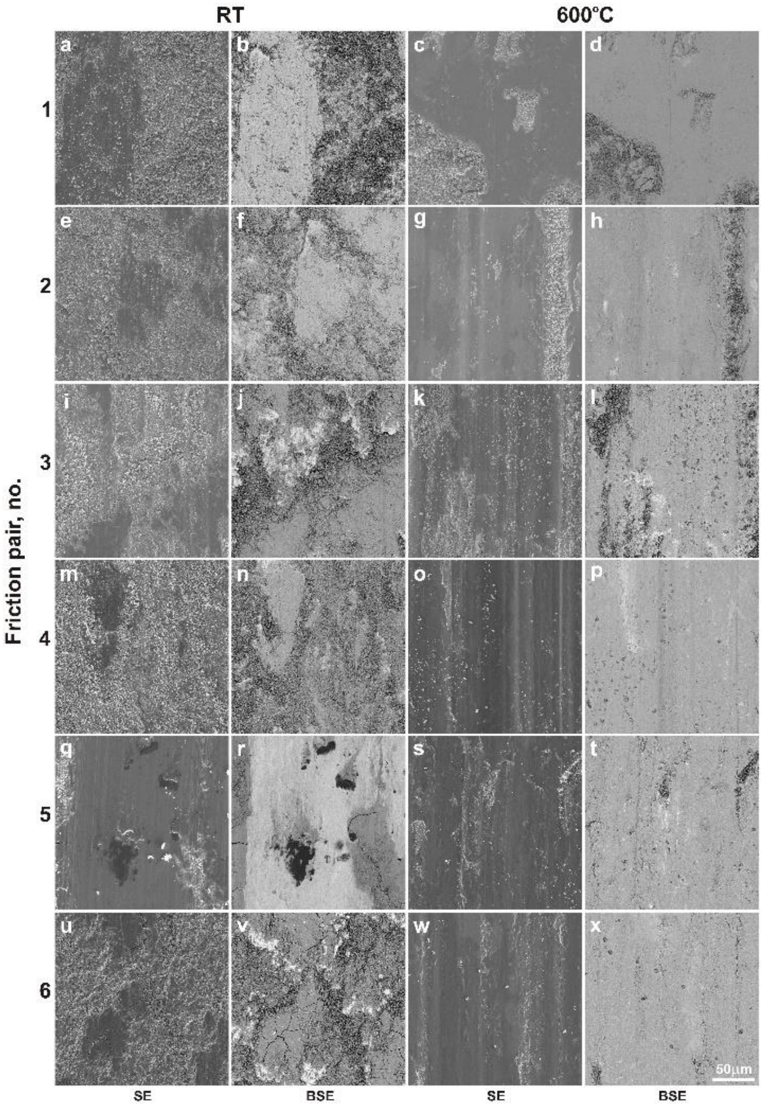

Worn surface of sinters.

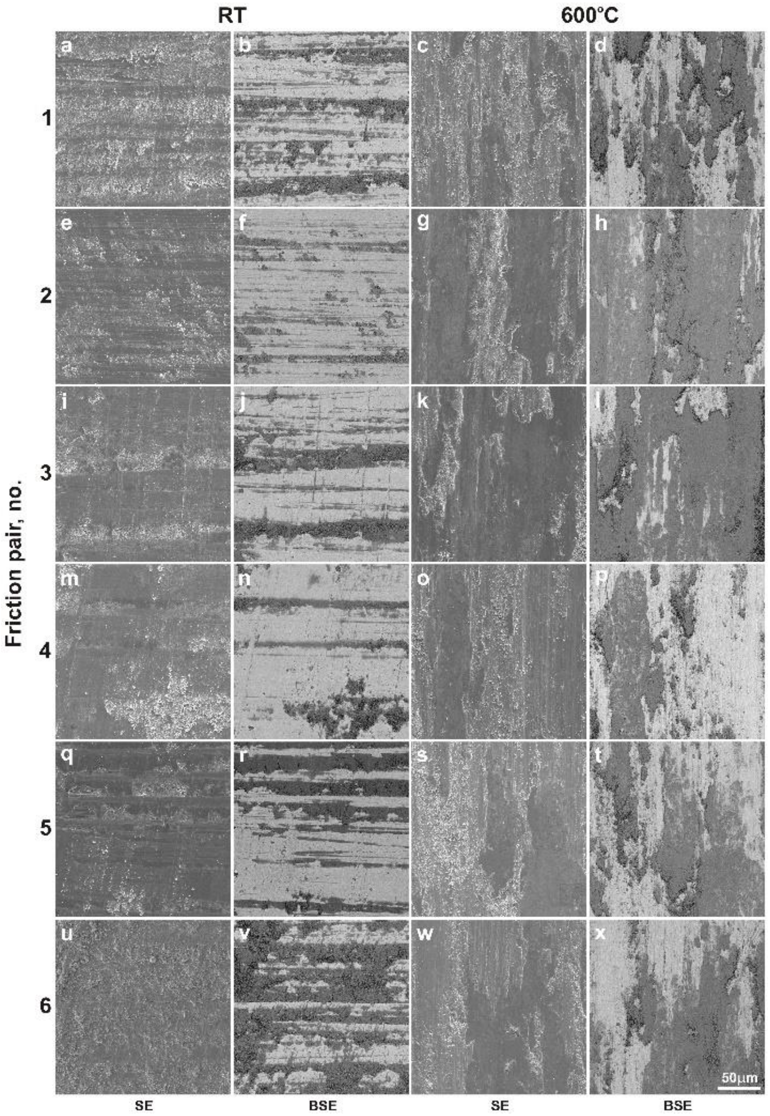

Worn surface of counter-specimens.

Piasecki A., Paczos P., Tuliński M., Kotkowiak M., Popławski M., Jakubowicz M., Boncel S., Marek A.A., Buchwald T., Gapiński B., Terzyk A.P., Korczeniewski E., Wieczorowski M., Microstructure, mechanical properties and tribological behavior of Cu-nano TiO_2-MWCNTs composite sintered materials. Wear 2023, vol. 522, s. 204834-1-204834-16

1 (Cu), 2 (Cu-1% CNTs), 3 (Cu-5% TiO_2), 4 (Cu-10% TiO_2), 5 (Cu-1% CNTs-5% TiO_2), 6 (Cu-1% CNTs-10% TiO_2)

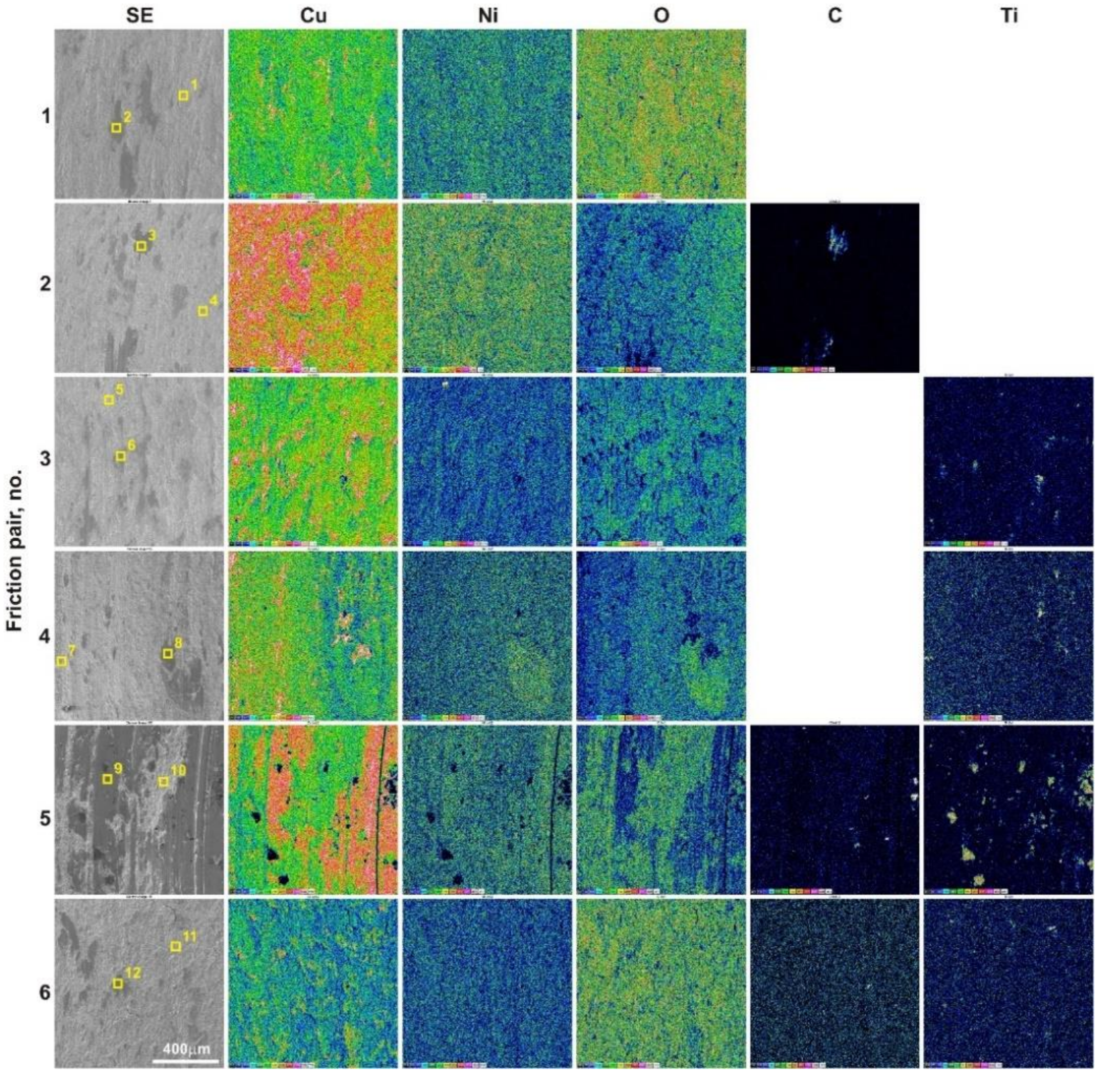

EDS maps of element concentration distributions on the sinter surface after friction wear test at room temperature.

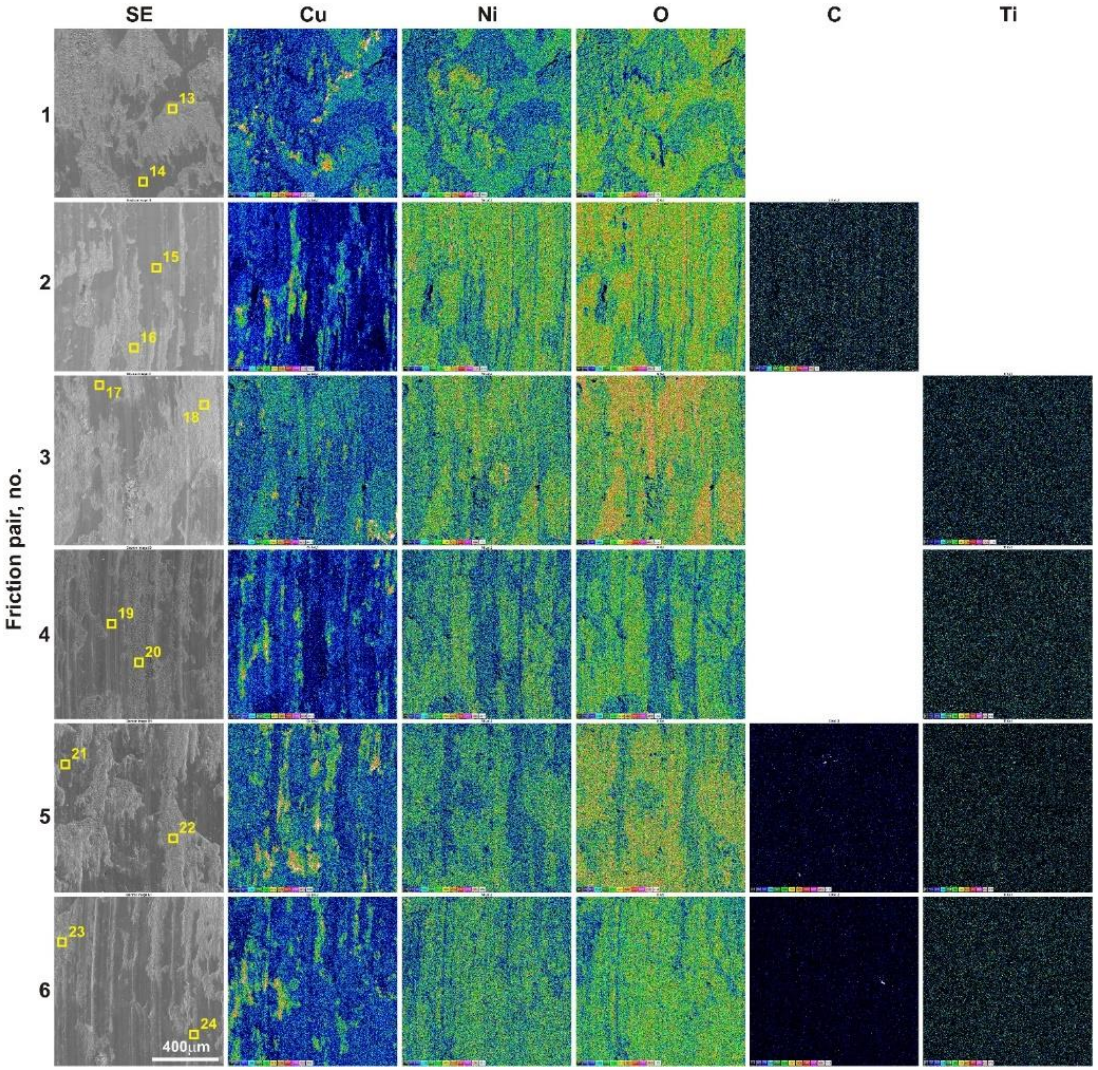

EDS maps of element concentration distributions on the sinter surface after friction wear test at 600°C.

Piasecki A., Paczos P., Tuliński M., Kotkowiak M., Popławski M., Jakubowicz M., Boncel S., Marek A.A., Buchwald T., Gapiński B., Terzyk A.P., Korczeniewski E., Wieczorowski M., Microstructure, mechanical properties and tribological behavior of Cu-nano TiO_2-MWCNTs composite sintered materials. Wear 2023, vol. 522, s. 204834-1-204834-16

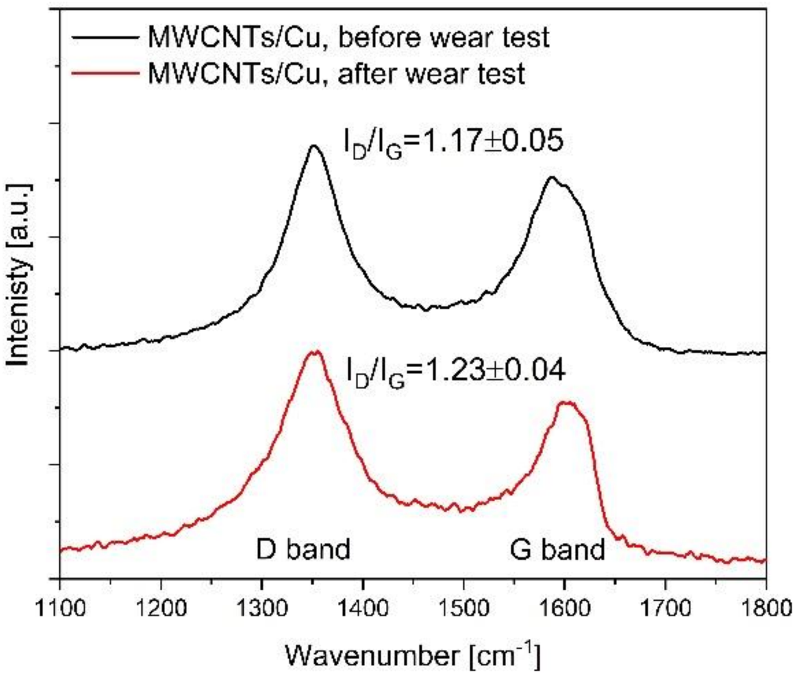

Raman spectra of MWCNTs before and after wear test.

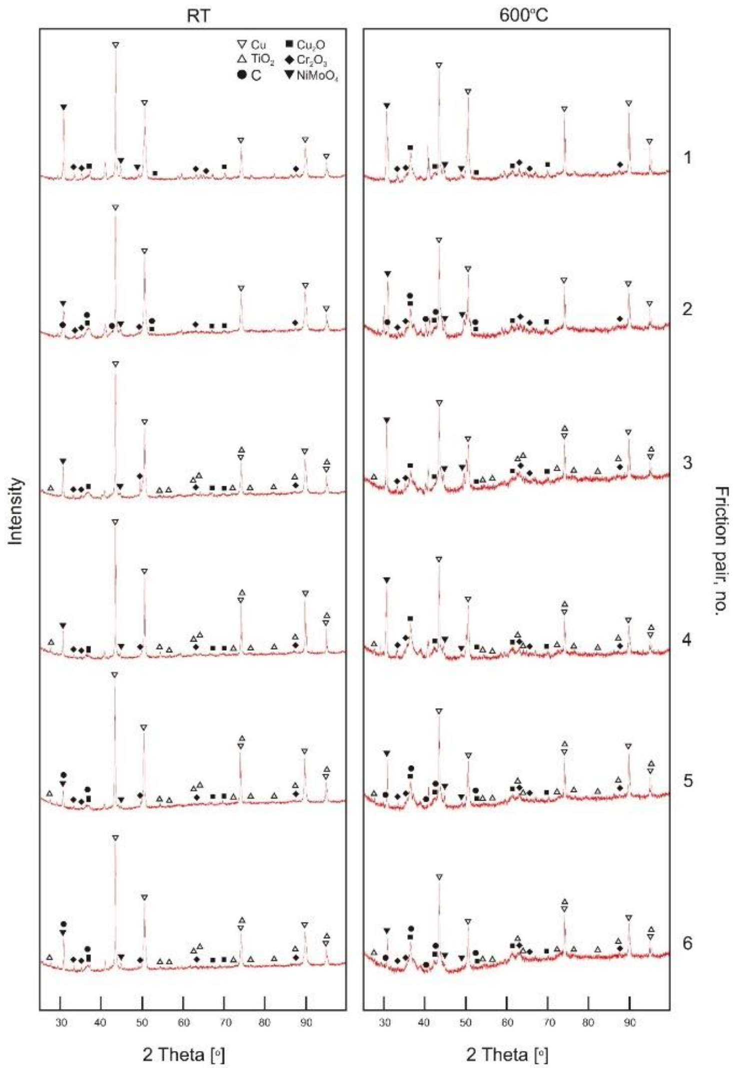

XRD patterns of worn surfaces.

1 (Cu), 2 (Cu-1% CNTs), 3 (Cu-5% TiO_2), 4 (Cu-10% TiO_2),
5 (Cu-1% CNTs-5% TiO_2), 6 (Cu-1% CNTs-10% TiO_2)

Piasecki A., Paczos P., Tuliński M., Kotkowiak M., Popławski M., Jakubowicz M., Boncel S., Marek A.A., Buchwald T., Gapiński B., Terzyk A.P., Korczeniewski E., Wieczorowski M., Microstructure, mechanical properties and tribological behavior of Cu-nano TiO_2-MWCNTs composite sintered materials. Wear 2023, vol. 522, s. 204834-1-204834-16

1 (Cu), 2 (Cu-1% CNTs), 3 (Cu-5% TiO_2), 4 (Cu-10% TiO_2), 5 (Cu-1% CNTs-5% TiO_2), 6 (Cu-1% CNTs-10% TiO_2)

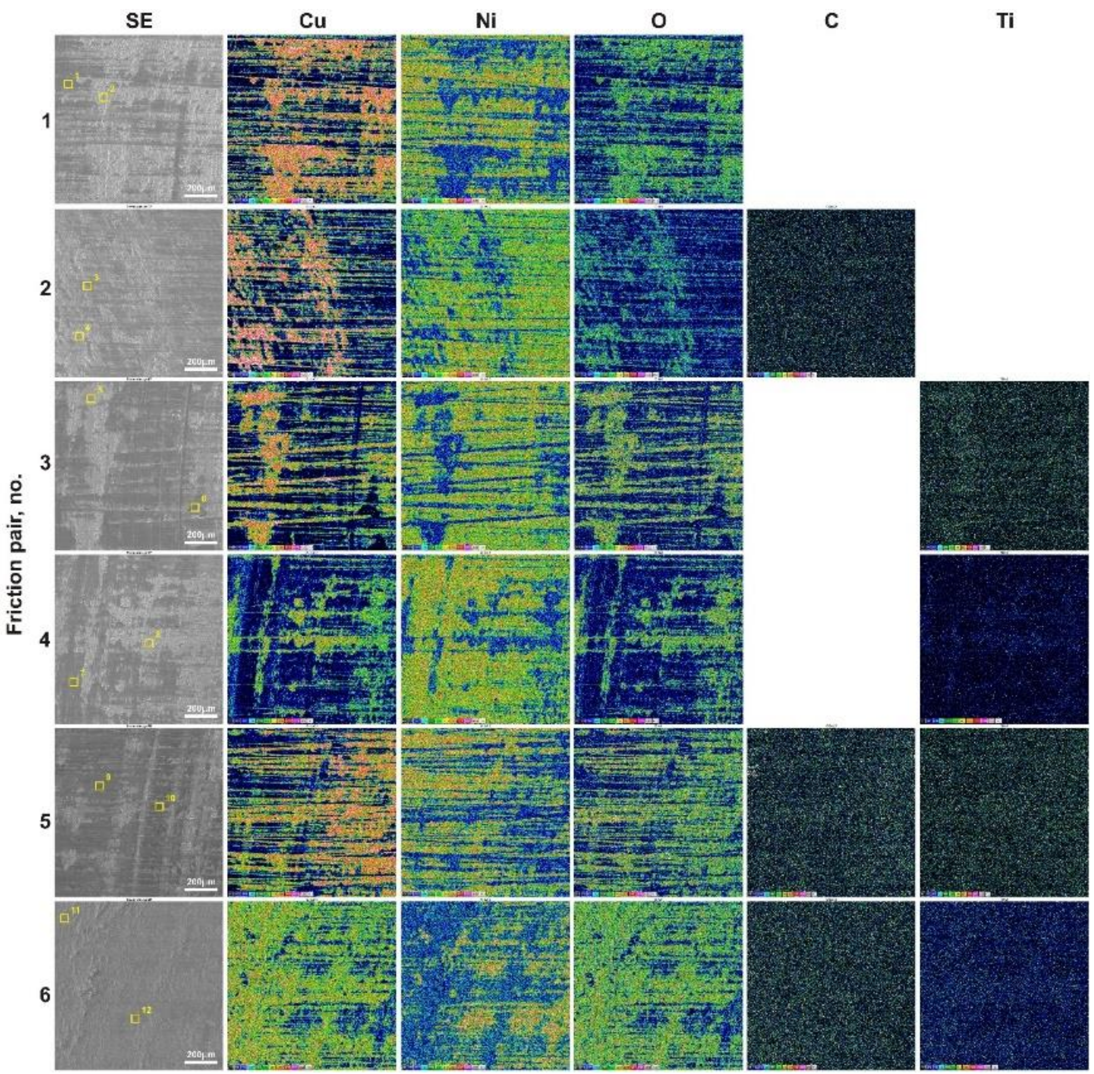

EDS maps of element concentration distributions on the Inconel®625 surface after friction wear test at room temperature.

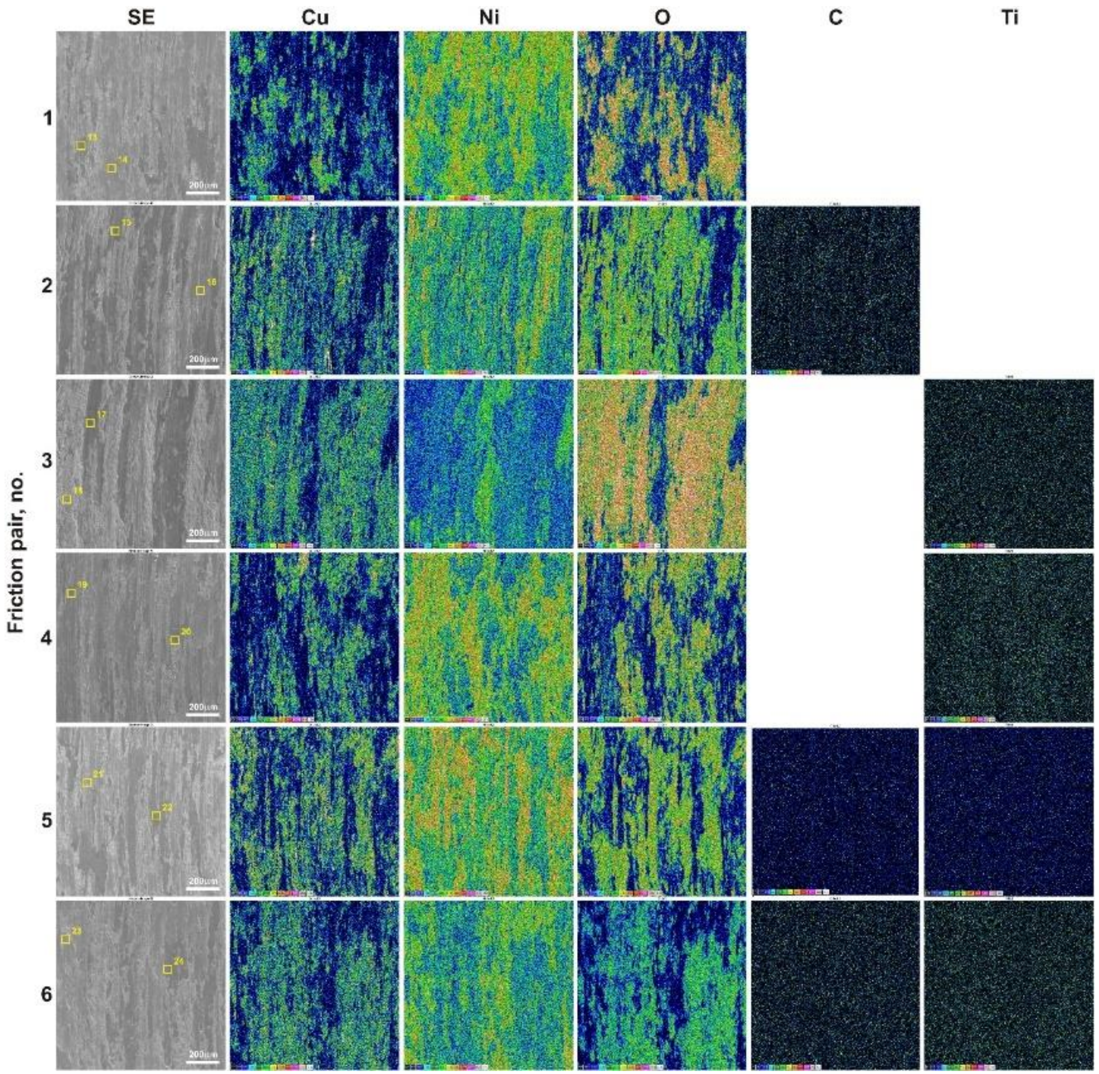

EDS maps of element concentration distributions on the Inconel®625 surface after friction wear test at 600°C.

Piasecki A., Paczos P., Tuliński M., Kotkowiak M., Popławski M., Jakubowicz M., Boncel S., Marek A.A., Buchwald T., Gapiński B., Terzyk A.P., Korczeniewski E., Wieczorowski M., Microstructure, mechanical properties and tribological behavior of Cu-nano TiO_2-MWCNTs composite sintered materials. Wear 2023, vol. 522, s. 204834-1-204834-16

Surface topography measurements; counter-specimen.

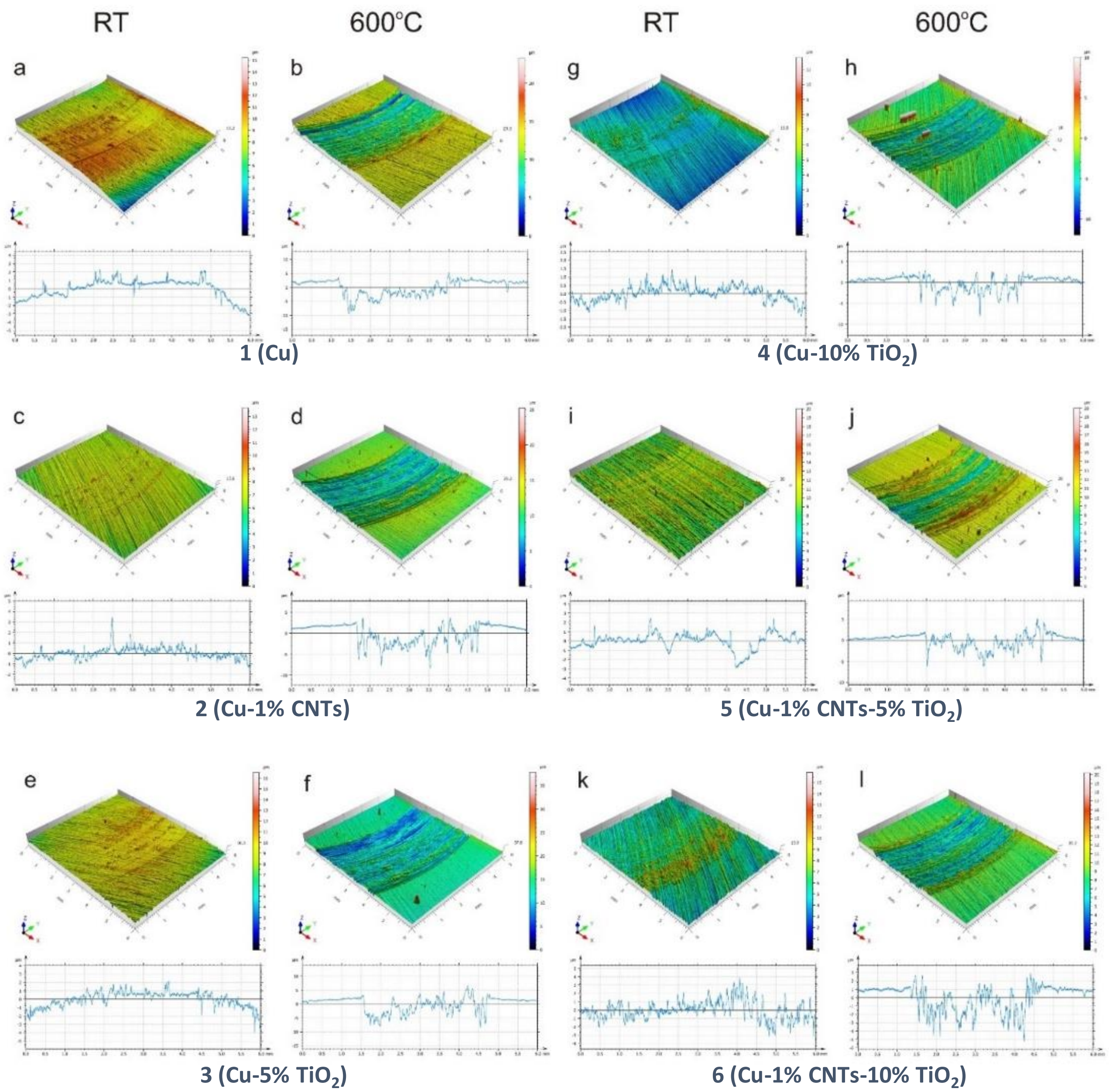

Piasecki A., Paczos P., Tuliński M., Kotkowiak M., Popławski M., Jakubowicz M., Boncel S., Marek A.A., Buchwald T., Gapiński B., Terzyk A.P., Korczeniewski E., Wieczorowski M., Microstructure, mechanical properties and tribological behavior of Cu-nano TiO_2-MWCNTs composite sintered materials. Wear 2023, vol. 522, s. 204834-1-204834-16

1 (Cu), 2 (Cu-1% CNTs), 3 (Cu-5% TiO_2), 4 (Cu-10% TiO_2),
5 (Cu-1% CNTs-5% TiO_2), 6 (Cu-1% CNTs-5% TiO_2)

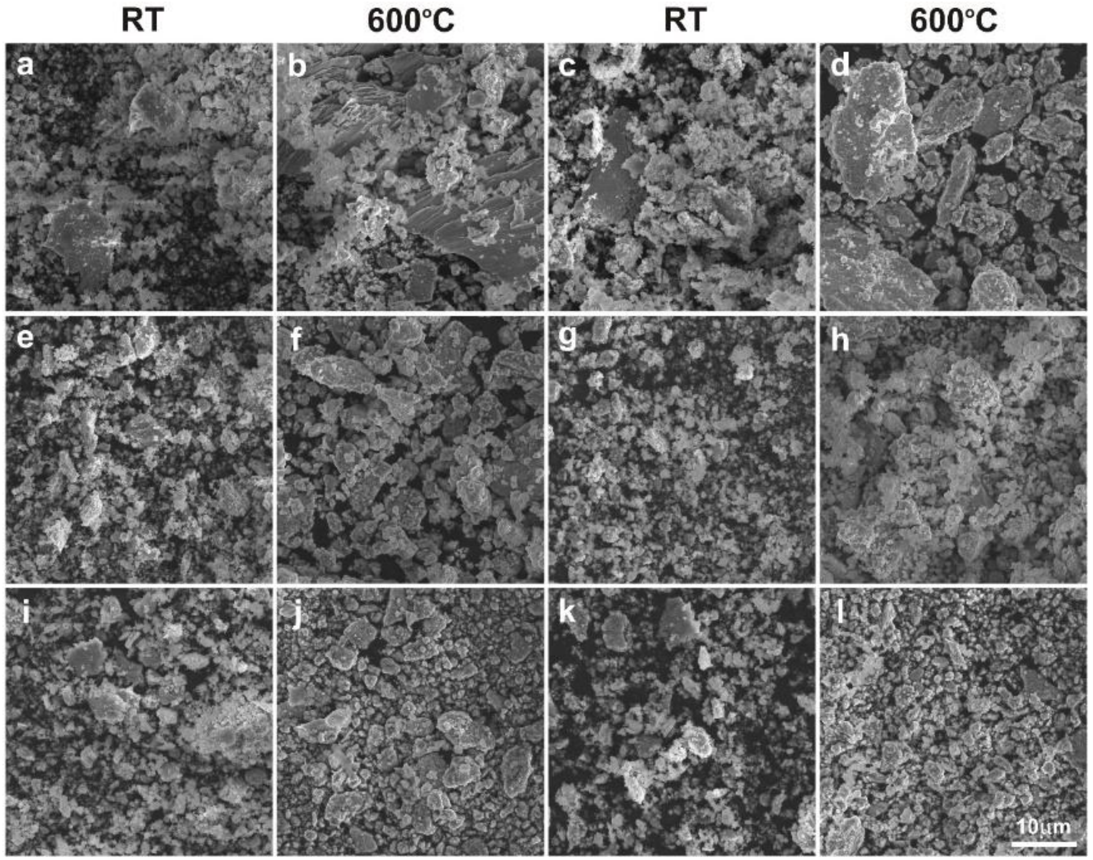

Worn debris.

The chemical composition of worn debris.

Friction pair no.	1		2		3		4		5		6	
Temperature	23°C	600°C	23°C	600°C	23°C	600°C	23°C	600°C	23°C	600°C	23°C	600°C
Cu	64.4	30.4	83.4	31.4	76.0	34.6	63.3	41.1	67.4	40.0	57.2	43.5
Ni	9.9	33.4	0.8	33.7	1.3	30.0	7.5	24.6	4.6	24.3	8.3	21.4
O	19.7	15.6	15.0	15.2	19.5	16.2	20.5	17.2	22.9	19.5	26.3	19.2
Cr	3.5	12.4	0.3	12.2	0.6	11.2	2.7	9.0	1.5	9.3	2.8	8.0
Mo	1.3	4.1	0.2	3.7	0.1	3.6	1.1	2.6	0.6	2.9	1.0	2.6
Nb	0.6	1.8	0.2	1.5	0.0	1.4	0.4	1.1	0.2	1.1	0.6	1.1
Fe	0.7	2.4	0.2	2.3	0.2	2.2	0.6	1.8	0.5	1.9	0.4	1.6
Ti					2.3	0.7	3.9	2.6	2.3	0.9	3.5	2.7

Piasecki A., Paczos P., Tuliński M., Kotkowiak M., Popławski M., Jakubowicz M., Boncel S., Marek A.A., Buchwald T., Gapiński B., Terzyk A.P., Korczeniewski E., Wieczorowski M., Microstructure, mechanical properties and tribological behavior of Cu-nano TiO_2-MWCNTs composite sintered materials. Wear 2023, vol. 522, s. 204834-1-204834-16

Thank you for your attention

The production of self-lubricating wear-resistant materials containing solid lubricants can be one of the most effective and economical methods to increase the durability of machine and vehicles parts.

adam.piasecki@put.poznan.pl